AD-A076 151 AVCO SYSTEMS DIV WILMINGTON MA F/G 11/2
IMPROVING THE STRESS RUPTURE AND CREEP OF SILICON NITRIDE.(U)
MAR 79 T T VASILOS , R M CANNON, B J WUENSCH NAS-3-20088
UNCLASSIFIED NASA-CR-159585 NL

| OF |
AD
A076151

END
DATE
FILMED
11-79
DDC

LEVEL II

NASA-CR-159585

IMPROVING THE STRESS RUPTURE AND CREEP OF SILICON NITRIDE

By

T. Vasilos
M. Cannon, Jr.
B.J. Wuensch

Avco Systems Division
201 Lowell Street
Wilmington, Massachusetts 01887

March 30, 1979

Final Rept.

Prepared for

National Aeronautics and Space Administration
NASA Lewis Research Center
Cleveland, Ohio 44135

Contract NAS-3-20088

FINAL REPORT

1. Report No. NASA-CR-159585	2. Government Accession No.	3. Recipient's Catalog No.
4. Title and Subtitle IMPROVING THE STRESS RUPTURE AND CREEP OF SILICON NITRIDE		5. Report Date March 30, 1979 6. Performing Organization Code 4461
7. Author(s) T. Vasilos, R.M. Cannon, and B.J. Wuensch		8. Performing Organization Report No. 10. Work Unit No.
9. Performing Organization Name and Address Avco Corporation, Systems Division Wilmington, MA. 01887		11. Contract or Grant No. NAS-3-20088
12. Sponsoring Agency Name and Address National Aeronautics and Space Administration Washington, D.C. 20546		13. Type of Report and Period Covered Contractor Report 14. Sponsoring Agency Code

15. Supplementary Notes

Project Manager, W.A. Sanders, Materials & Structures Division
NASA Lewis Research Center
Cleveland, Ohio

16. Abstract

Yttria-stabilized zirconium oxide (Zyttrite) additions to purified silicon nitride were found to improve the high temperature strength, stress rupture and creep properties of hot pressed samples very markedly.

Room temperature bend strengths, however, of four (4) compositions evaluated were each about one-third lower than Norton Company's NC-132 silicon nitride composition. This difference decreased with increasing temperature until at 1200°C, there was reasonable equivalence between most of the zyttrite containing compositions and NC-132 in terms of short time bend strength measurements.

At 1370°C, the 10 and 20 wt. % containing zyttrite compositions showed bend strengths as much as double the NC-132 material.

Bend stress rupture results for 10 and 20 wt. % zyttrite containing compositions showed a strong stress sensitivity at the 276 MN/m^2 (40 Kpsi) level above 1200°C.

Creep in bending measurements showed that at 1370°C and 1450°C, zyttrite containing compositions exhibited creep rates that were about 2 orders of magnitude lower than NC-132 material samples.

All compositions appeared to follow deformation kinetics related to a visco-elastic mechanism, i.e., glassy phase diffusional creep or grain boundary sliding.

17. Key Words (Suggested by Author(s))	18. Distribution Statement
Turbine materials Creep rate Ceramics Silicon Nitride Stress rupture Bend Strength	Unclassified - Unlimited

19. Security Classif. (of this report)	20. Security Classif. (of this page)	21. No. of Pages	22. Price*
Unclassified	Unclassified	67	3.00

* For sale by the National Technical Information Service, Springfield, Virginia 22161

NASA-C-168 (Rev. 10-75)

FOREWORD

The research work described herein was conducted by the Avco Corporation, Systems Division, under NASA Contract NAS3-20088. The work was performed under the management of the NASA Project Manager, Mr. William A. Sanders, Materials and Structures Division, NASA/Lewis Research Center. Dr. Thomas Vasilos was the Avco Project Leader with Dr. Rowland M. Cannon, and Dr. B.J. Wuensch assisting in Materials Evaluation. Other Avco personnel who contributed significantly to this project were Ernest Vallante, Burton MacAllister and George Ross.

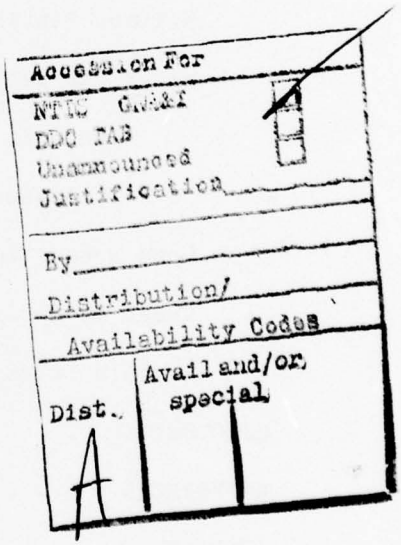

TABLE OF CONTENTS

LIST OF ILLUSTRATIONS

LIST OF ILLUSTRATIONS (Cont'd)

LIST OF ILLUSTRATIONS (Concl'd)

LIST OF TABLES

SUMMARY

The objective of this program was to improve the stress rupture and creep properties of silicon nitride through the use of a yttrium-stabilized zirconium oxide additive (Zyttrite). The range of additive concentration studied was 10 to 25 wt. % in 5% increments, and Norton NC-132 grade of silicon nitride was also studied for comparison purposes.

A special batch of high purity silicon nitride was produced for the program by AME of England. Although the powder supplied had a very high iron concentration, it was found that much of the iron content was removed by filtering the powder through 15 μm filters, a step originally employed to eliminate large inclusions and agglomerates.

Dense billets of four (4) silicon nitride-zyttrite compositions were prepared by unidirectional hot pressing techniques employing graphite dies. The compositions were evaluated in terms of transverse bend strength, from room temperature to 1370°C, bend stress rupture from 1200 to 1370°C, and two of the most promising compositions were selected for creep in bending measurements. These were the 10 and 20 wt. % Zyttrite additive compositions. Norton NC-132 material was also evaluated under these test conditions. A limited number of stress rupture tests were also performed in tension on the 10 wt. % Zyttrite containing composition as well as on NC-132.

On a comparative basis, the results show the NC-132 material to be stronger than the Zyttrite containing compositions in terms of short-time transverse bend strength measurements up to about 1285°C. However, at 1370°C, the best Zyttrite-containing compositions reveal bend strengths about double that of NC-132 material. This has been attributed to the more refractory nature of the zirconium oxynitride phase, that has been identified in the Zyttrite-containing compositions, as compared to the existence of a lower temperature stable "glassy" phase in the NC-132 material.

Bend stress rupture and creep experiments also reveal the superior high temperature properties of the Zyttrite-containing compositions. For comparable levels of stress, the creep resistance of the Zyttrite-containing material was about two orders of magnitude greater.

INTRODUCTION

The objective of this program was to improve the stress rupture and creep properties of silicon nitride. The approach was to enhance these properties through incorporation of a yttrium-stabilized zirconium oxide additive (known as Zyttrite) to a specially prepared grade of high purity silicon nitride.

Earlier work[1] had shown that yttrium-stabilized zirconia additions, in the form of a high purity, fine particulate had very significant effects in raising both the short term low temperature bend strengths as well as the high temperature strengths. In addition, the best stress rupture behavior was observed with samples containing the zirconia additive. This was consistent with both low and higher purity grades of silicon nitride powder. An important aspect of the current program was to determine whether an optimum concentration of zirconia additive exists in this system in terms of overall properties. Four powder compositions were selected containing 10, 15, 20 and 25 weight percent zirconium oxide.

Samples were characterized at stages before and after evaluation to reveal composition, microstructure and possible failure modes and mechanisms.

The silicon nitride-zirconia materials developed and evaluated in the program were rated against each other as well as Norton NC-132 grade silicon nitride.

Powder Characterization and Processing

Characterization

Advanced Materials Engineering, Ltd., was placed under subcontract to produce a 22.7 kgs (50 lbs.) batch of high purity silicon nitride powder containing no more than the following amounts of impurity elements (in wt. %): 1.6 oxygen, 0.24 carbon, 0.04 calcium, 0.005 sodium, 0.005 potassium, 0.065 iron, 0.12 aluminum and 0.008 magnesium. The powder was to consist

of at least 80% alpha phase with the remainder of the powder consisting of the beta phase; no other compounds were to be identified by x-ray diffraction analysis.

In addition, two kgs (4.4 lbs.) of Zyttrite-6 (zirconium dioxide stablized by 6 mole percent yttrium oxide) were obtained from the HTM Company of Cincinnati, Ohio.

Table I provides chemical analysis for the as-received silicon nitride powder as determined by spectrochemical and wet chemical analysis.

Except for the iron content which was found to be very excessive, the analysis revealed that the powder as supplied was within specification. The vendor analysis for iron indicated a content of 0.17 percent.

Since the powder was obtained on a best effort basis, there was no recourse but to proceed with the program using this silicon nitride. (As it turned out, filtering the powder through a 15 μm filter did significantly reduce the iron content.)

Particle and agglomerate structure analyses were performed for both the silicon nitride and zyttrite powders. Scanning electron microscopy revealed a characteristic plate-like particle structure for the silicon nitride, with particle diameters ranging from about .1 μm to .9 μm. A Coulter Counter analysis revealed a median size of 1.9 μm and particulates ranging up to about 25 μm. The discrepancy probably results from the highly agglomerated nature of this powder, whereby the individual particles were not entirely dispersed in aqueous or alcoholic media.

Scanning electron microscopy of the Zyttrite powder revealed a strongly agglomerated structure as well. The agglomerates ranged from 0.1 to 1 μm in diameter. The individual crystallite particles were closer to 0.01 μm.

TABLE I

CHEMICAL ANALYSIS OF AS-RECEIVED SILICON NITRIDE POWDER

Element	Maximum Permitted Concentration (wt. %)	Concentration Determined (wt. %)
Calcium	0.04	0.03
Iron	0.065	0.39 ± .04
Aluminum	0.12	0.085 ± .009
Magnesium	0.008	.0008 ± .0008
Sodium	0.005	< 0.001
Potassium	0.005	< 0.001
Carbon	0.24	0.28 ± .03
Antimony	-	< 0.003
Manganese	-	0.001
Nickel	-	< 0.01
Chromium	-	0.02
Cobalt	-	< 0.01
Copper	-	0.02
Oxygen	1.6	1.4

Coulter Counter analysis revealed a median size of 4.5 μm, which again was a measure of the agglomerate structure which ranged to about 25 μm as well.

Figures 1 and 2 are scanning electron micrographs of as-received silicon nitride and Zyttrite particulates.

Surface area measurements for each of these powders reveal 17 m^2/gm for Si_3N_4 and 60 m^2/gm for the Zyttrite. X-ray diffraction analysis of the as-received silicon nitride revealed an alpha phase content of 87 wt. % and a beta phase content of 13%. A trace of silicon oxynitride phase was also noted. No other phases were apparent and the analysis approximates that given for the 9-5 lot of powder used in the earlier program.

Powder Processing

Classification

Experiments were conducted to classify the silicon nitride powder and to separate out particles larger than 10 μm in diameter. The powder is highly agglomerated and difficulties were experienced immediately when an Alpine Air Classifier unit was employed.

A very low yield of ~1% was obtained through the 10 μm filter and this was improved only slightly when a 20 μm filter was used. A reasonable yield was obtained only when a 44 μm filter screen was employed. In view of the unacceptability large size of the 44 μm filter, it was decided to study the effectiveness of a liquid dispersionfiltration process.

A unit similar to the one employed by D.J. Shanefield and R.E. Mistler of Western Electric Company[2] was put together employing an electric pump. Filter cloth was obtained from the Tedko Co. of Elmsford, New York. Filters with 10 μm, 15 μm and 20 μm openings were obtained for the effort and each was tried. It was found that for a variety of pumping speeds and solids

30° Tilt 20,000X

Figure 1. Scanning Electron Micrograph of As-Received Silicon Nitride Powder.

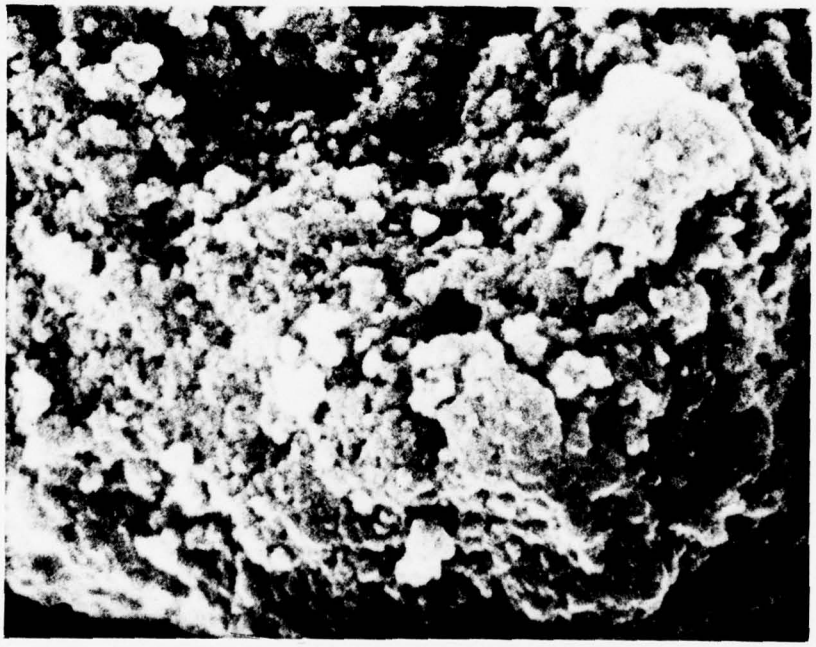

30° Tilt 20,000X

Figure 2. Scanning Electron Micrograph of As-Received Zyttrite Powder.

concentrations, a significant percentage of material ($\geq$50%) could be made to pass through the 15 μm filter. A very much lower yield was obtained through the 10 μm filter and it was decided to continue processing the powder through the 15 μm filter. A special peristaltic pump was then obtained to provide the proper pumping action required.

Both alcohol and distilled water were initially employed to disperse the powder and best results were obtained with the distilled water. A Coulter Counter analysis was performed on silicon nitride powder that had passed through the 15 μm filter set up. The sample was sonified and dispersed in an anionic wetting agent before counting. The distribution appeared to be bi-modal with the larger median around 1.75 μm and the smaller below 0.8 μm. Approximately 2 percent of the particles showed a size between 15 and 20 μm and these probably were agglomerates that were not broken up by the dispersion process.

A comparison of Coulter Counter results before and after filtration of the silicon nitride revealed that the 5 percent fraction of particulates in the 20-25 μm range was eliminated. Further, a bi-modal size distribution became apparent after filtration, which was not evident before, where the median size was 1.9 μm. Figure 3 is a scanning electron micrograph of filtered silicon nitride powder and reveals a uniform agglomerate structure.

An x-ray diffraction analysis performed on filtered silicon nitride powder revealed no significant difference from the unclassified powder. The alpha phase content was found to be 88 percent and the beta phase content was 12 percent. A trace line for silicon oxynitride was somewhat stronger than for the unclassified material.

A surface area measurement for the filtered silicon nitride powder showed a value of 19 m^2/gm, or about 10 percent higher than the unclassified powder.

Figure 3. Scanning Electron Micrograph of Silicon Nitride Processed through 15 Micron Filter.

Chemical analyses were performed on silicon nitride powder that had passed through the 15 μm filter set-up and also on a sample of milled 20% Zyttrite-80% silicon nitride mix. The latter was taken from a batch that had been ball-milled in a polyethylene container with methyl alcohol and tungsten carbide balls for a time period of 16 hours. The results are provided in Table II and are compared with earlier analyses on the as-received silicon nitride powder.

Filtering through the 15 μm filter appears to reduce the iron concentration to within 300 ppm of the specification level. Aside from an increase in oxygen content, no significant increase in other impurity was detected. In fact, a slight decrease in a number of impurities was observed. The ball-milled batch shows a significant pick-up of tungsten and nickel content, i.e., better than a factor of six times. The tungsten concentration is still low overall at no more than 100 ppm, but the nickel concentration now has approached the iron content. The source of the conaminant is undoubtedly the nickel-bonded tungsten carbide grinding media. To reduce the degree of contamination, the milling time was reduced by one-half in future batch preparations. Oxygen content was increased as a result of filtering and drying, but the level was not considered excessive. Carbon content appeared to have remained steady throughout the particulate processing cycle. With the exception of the iron and oxygen analyses, there was reasonable compatibility in the analytical determinations obtained by the different laboratories.

Batch Preparation

Silicon nitride-zyttrite mixtures were blended by ball milling in polyethylene containers with tungsten carbide balls. Powder batches of

TABLE II

CHEMICAL ANALYSIS OF POWDERS

Element	Maximum Permitted Conc. for As-Received Si_3N_4 (Wt. %)	Vendor Analysis for As-Received Si_3N_4 (Wt. %)	Contractor Analysis for As-Received Si_3N_4 (Wt. %)	NASA/Lewis Lab Analysis for As-Received Si_3N_4 (Wt. %)	Contractor Analysis of Filtered Si_3N_4 Thru 15 μm (Wt. %)	Contractor Analysis of Ball-Milled Batch 20 ZrO_2-80 Si_3N_4 (Wt. %)
Calcium	0.04		0.03	0.022	0.03	0.003-0.03
Iron	0.065	0.17	(0.2-0.39 wet chem.)	{0.11 spec. 0.18 wet chem.	0.095	0.075
Aluminum	0.12		0.085 ± .009	0.076	< 0.10	.1
Magnesium	0.008		0.0008 ± .00008		< 0.003	0.006
Sodium	0.005		< 0.001	0.007	< 0.002	0.004
Potassium	0.005		< 0.001		< 0.002	0.004
Carbon	0.24		0.28 ± .03	0.234	0.27	0.29
Oxygen	1.6		1.4	1.11	1.8	
Antimony			< 0.003			
Manganese			0.001		0.001	0.001-0.01
Nickel			< 0.01		< 0.01	.060
Chromium			0.02		< 0.03	0.003-0.03
Cobalt			< 0.01		0.001	0.001-0.01
Cooper			0.02		< .003	0.0003-0.003
Tungsten					.001	.005-.01

approximately 250-300 gms were wet-milled with methyl alcohol disperant. Initial milling time was 16 hours, but this was changed to 8 hours to reduce the nickel contaminant from 0.060 percent to .035 percent. The wet mixtures were oven-dried below 100°C and the dried crust broken up with spatulas prior to loading into graphite dies for hot pressing.

Scanning electron micrographs for each of the four silicon nitride-zyttrite compositions as blended powders are provided in Figures 4-7 and each micrograph reveals rather uniform agglomerate size of less than five microns.

Billet Fabrication

Dense samples of the various silicon nitride-zyttrite compositions were prepared by unidirectional hot pressing techniques employing graphite dies. The conditions and results are reported in Table III. The billet size was 5.08 cm x 5.08 cm x 1.27 cm (2" x 2" x 1/2").

These billets were used as stock material for the preparation of bend test specimens.

Billet 1959 and 1960 were fabricated later on in the program as stock material for bend stress rupture testing, when it was determined that the 10 and 20 wt. percent zyttrite compositions appeared most promising for follow-up testing.

Densification time plots for particular billets are provided in Figure 8.

Overall, the densification kinetics for the four zyttrite containing compositions are similar. But, the initial slope of the 1800°C isothermal range part of the plots show densification rate to increase with increasing zyttrite concentrations. Approximately 15 percent of the preform porosity was removed during the initial stage to 1800°C; at 1800°C, approximately 30 minutes or less was required to reach about 3% residual porosity (closed

Figure 4. Scanning Electron Micrograph of Blended Silicon Nitride-10 Wt. % Zyttrite Powder.

Figure 5. Scanning Electron Micrograph of Blended Silicon Nitride-15 Wt. % Zyttrite Powder.

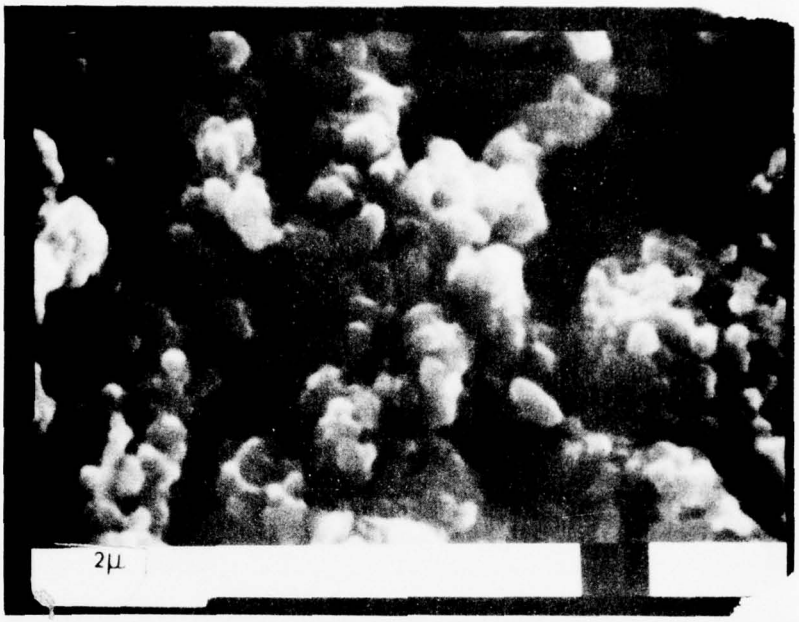

Figure 6. Scanning Electron Micrograph of Blended Silicon Nitride-20 Wt. % Zyttrite Powder.

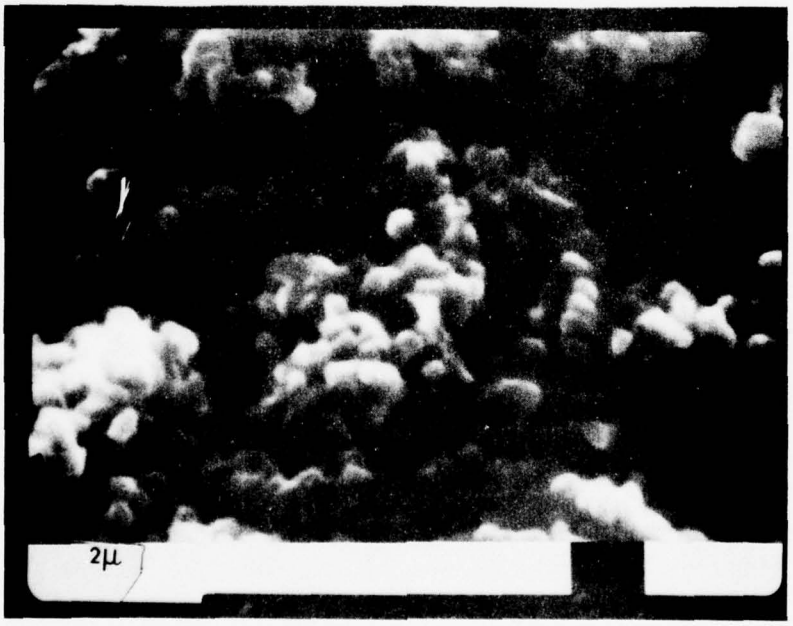

Figure 7. Scanning Electron Micrograph of Blended Silicon Nitride-25 Wt. % Zyttrite Powder.

TABLE III

SILICON NITRIDE BILLET FABRICATION CONDITIONS AND RESULTS

Run No.	Material	Additive	Temp. °C	Temp. °F	Pressure MN/m^2	Pressure psi	Time (min)	Density gm/cc	Grain Size μm
1936	AME Si_3N_4 thru 15 um	20 wt. % Zyttrite-6	1800	3272	27.5	4000	120	3.49	1-2
1937	" "	10 wt. % Zyttrite-6	1800	3272	27.5	4000	120	3.23	1-2
1938	" "	15 wt. % Zyttrite-6	1800	3272	27.5	4000	120	3.40	1-2
1939	" "	25 wt. % Zyttrite-6	1800	3272	27.5	4000	120	3.60	1-2
1940	" "	20 wt. % Zyttrite-6	1800	3272	27.5	4000	120	3.50	1-2
1942	" "	25 wt. % Zyttrite-6	1800	3272	27.5	4000	120	3.60	1-2
1959	" "	20 wt. % Zyttrite-6	1800	3272	27.5	4000	120	3.48	1-2
1960	" "	10 wt. % Zyttrite-6	1800	3272	27.5	4000	120	3.30	1-2
1963*	" "	20 wt. % Zyttrite-6	1800	3272	27.5	4000	120	3.54	1-3
1964*	" "	10 wt. % Zyttrite-6	1800	3272	27.5	4000	120	3.25	1-4
1965**	" "	20 wt. % Zyttrite-6	1800	3272	27.5	4000	120	3.48	4-6
1981**	" "	10 wt. %	1800	3272	27.5	4000	120	3.24	4-6

* Billets 1963 and 1964 were first prepared as lower density, undersized preforms and then forged into 2 1/4" x 2 1/4" cavities at conditions tabulated above.

** Billets 1965 and 1981, after hot pressing at conditions tabulated, were heat-treated to 1850°C for 8 hours to enlarge the grain structure.

Figure 2. DENSIFICATION VS. TIME PLOTS FOR THE FOUR COMPOSITIONS STUDIED

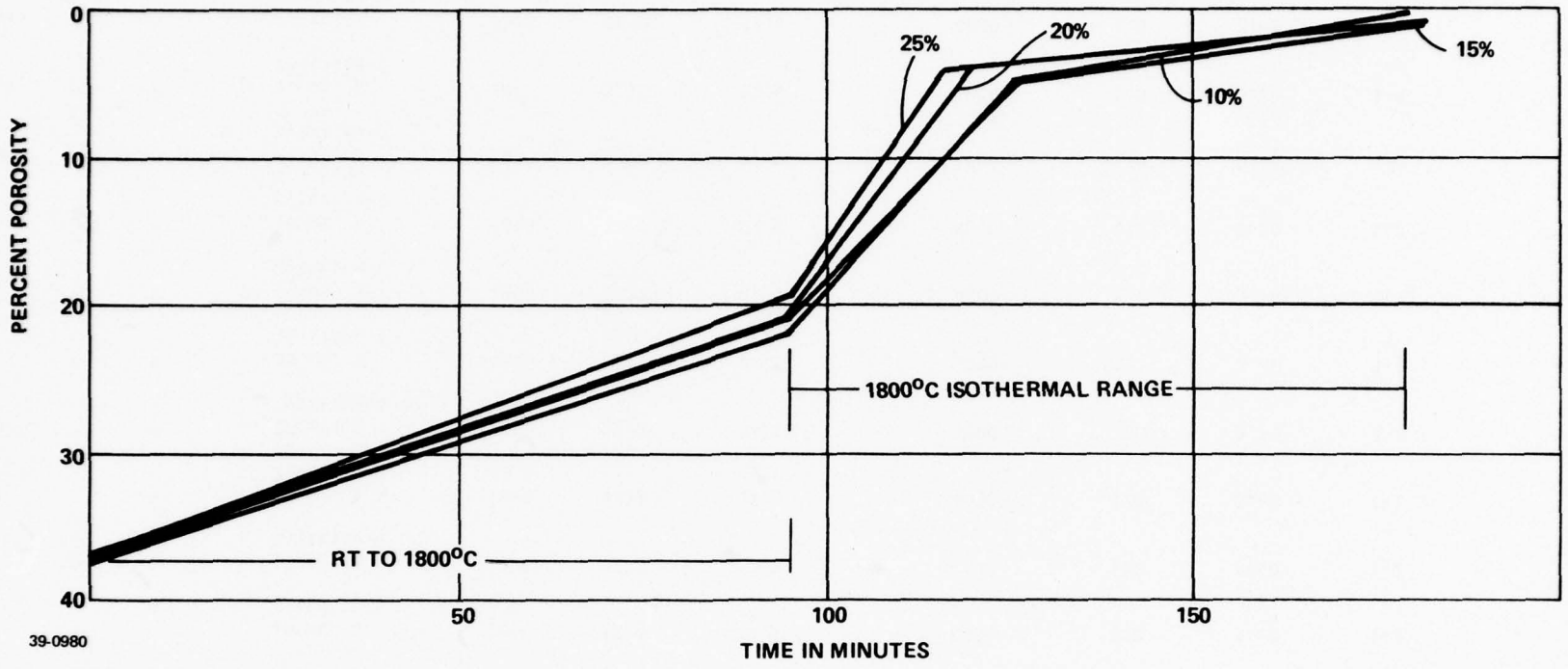

pore region) and approximately another hour was required to reach essentially full densification.

Billets 1963 and 1964 were first prepared as undersized preforms by hot pressing at 1750°C and 4000 psi and then forged in a 2 1/2" x 2 1/4" cavity die at 1800°C and 4000 psi. The thickness of the preform billet 1963 (20% zyttrite) was reduced from 1.004 cm (0.395 in.) to 0.635 cm (0.275 in.) and the final density was 3.54 g/cc. The thickness of the preform billet 1964 (10% zyttrite) was reduced from 1.27 cm (0.50 in.) to 0.889 cm (0.35 in.) and the final density was 3.25 g/cc.

Billets 1965 and 1981 were heat-treated after hot pressing to enlarge the grain structure. This was performed at 1850°C for 8 hours in a graphite furnace with flowing nitrogen gas.

Fabricated Billet Examination

Microscopy

Polished section photomicrographs are shown in Figures 9 to 12 for billets 1936, 1937, 1938, 1939 and 1940. These sections were taken parallel to the direction of pressing and were representative of each billet cross-section.

In general, the figures show dense microstructure with little or no apparent porosity. A high index of refraction iron silicide phase appears common in each billet with particle diameters largely in the 1 μm range and a few particles up to 5 μm in diameter. A zirconium oxynitride phase appears as the light gray phase (readily apparent in Figure 10 - Billet 1938 - 15 percent zyttrite) in a darker gray matrix of silicon nitride. The phase darker than the matrix in Figure 9 is porosity and in Figures 11 and 12 is probably silicon oxynitride.

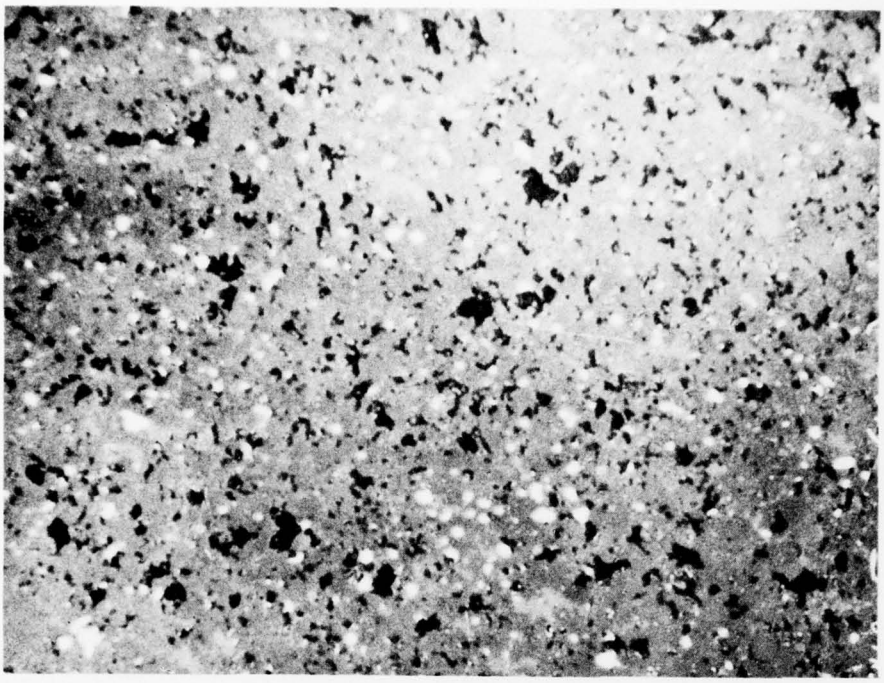

1000X

Figure 9. Microphotograph of Cross-Section of Billet 1937 (10% Zyttrite Additive).

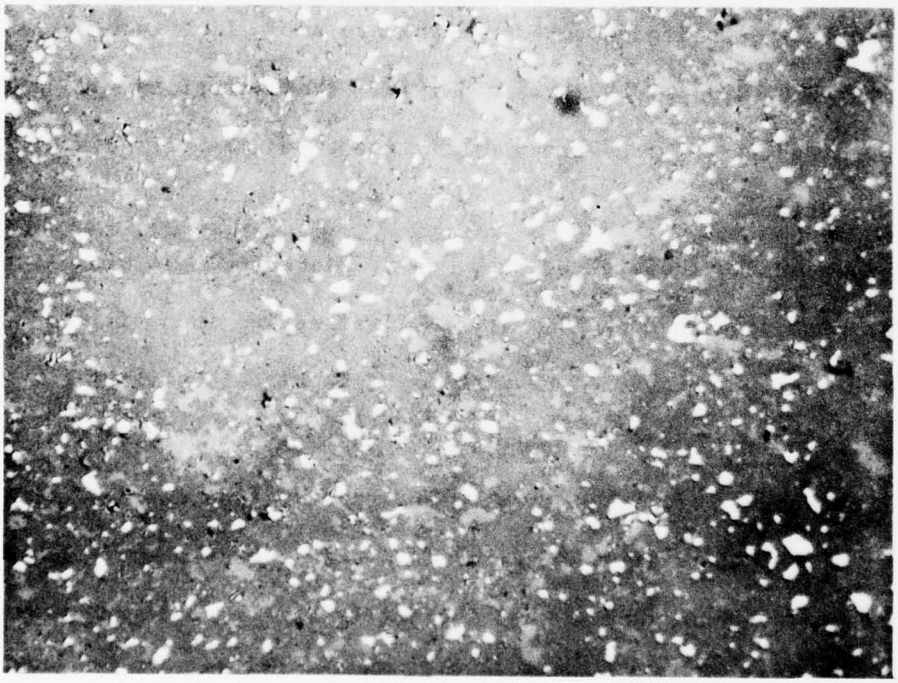

1000X

Figure 10. Microphotograph of Cross-Section of Billet 1938 (15% Zyttrite Additive).

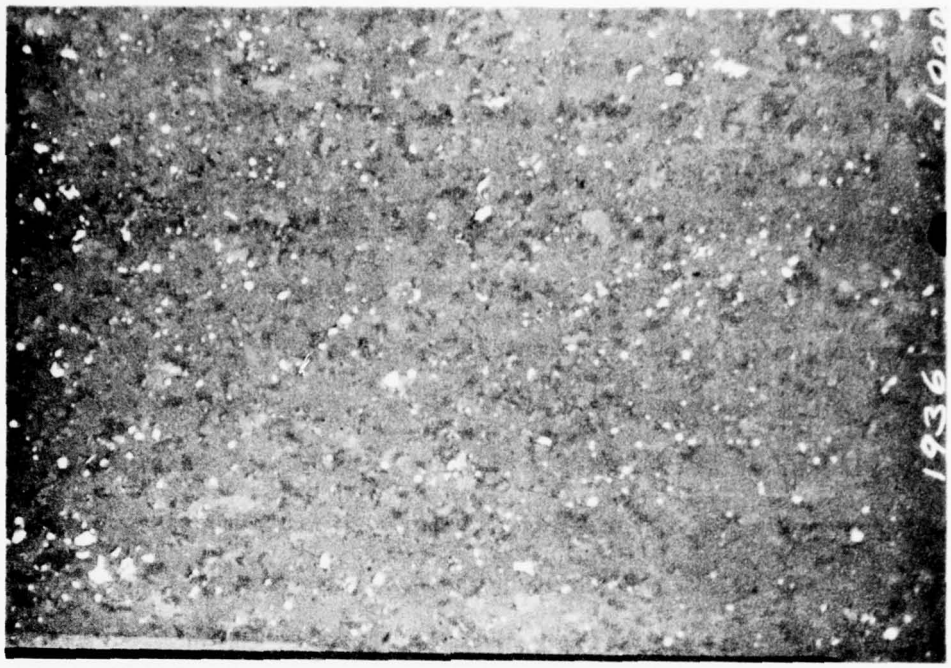

1000X

Figure 11. Microphotograph of Cross-Section of Billet 1936 (20% Zyttrite Additive).

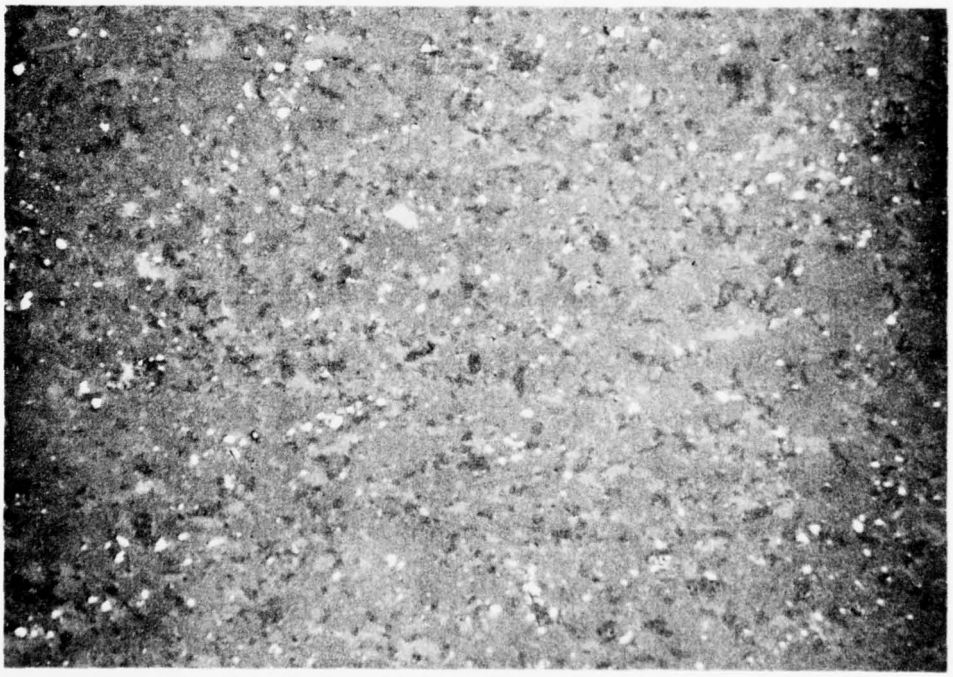

1000X

Figure 12. Microphotograph of Cross-Section of Billet 1939 (25% Zyttrite Additive).

A probe scan was performed on a zyttrite containing sample to verify zirconium content in the predominant second phase that appears in polished section micrographs. Figure 13 provides an SEM of a polished section taken from Billet No. 1942 (25 percent zyttrite additive). The light colored phase and the darker matrix were spot scanned for predominant chemistry and the results reveal silicon to be the dominant element in the matrix zone and zirconium, the dominant element in the lighter colored phase (arrows point to the two zones at which the analyses were performed in Figure 13).

Two billets of Norton NC-132 silicon nitride were obtained as one lot for purposes of comparative evaluation. Their dimensions were 5.1 cm x 5.1 cm x 1.27 cm thick. One billet was sectioned for microstructure examination and polished section photomicrographs are shown in Figures 14a and 14b. Figure 14 which shows surface sections parallel and perpendicular to the direction of pressing reveals no particular microstructure variation as a result of direction. The structure appears very dense (billet density of 3.2 g/cc and exhibits a relatively uniform distribution of an iron silicide phase and a silicon oxynitride phase which is darker than the matrix. In general, the size of the silicide phase approaches but is smaller than the size of the oxynitride phase. This is observed better at higher magnification as shown in Figure 15. In the field of view there is an occasional large inclusion particle of iron silicide as revealed in Figure 15b. The structure otherwise appears well-densified and quite uniform in phase distribution and phase size. Also, the iron silicide particle size in the NC-132 materials appears considerably smaller than for any of the zyttrite-silicon nitride compositions.

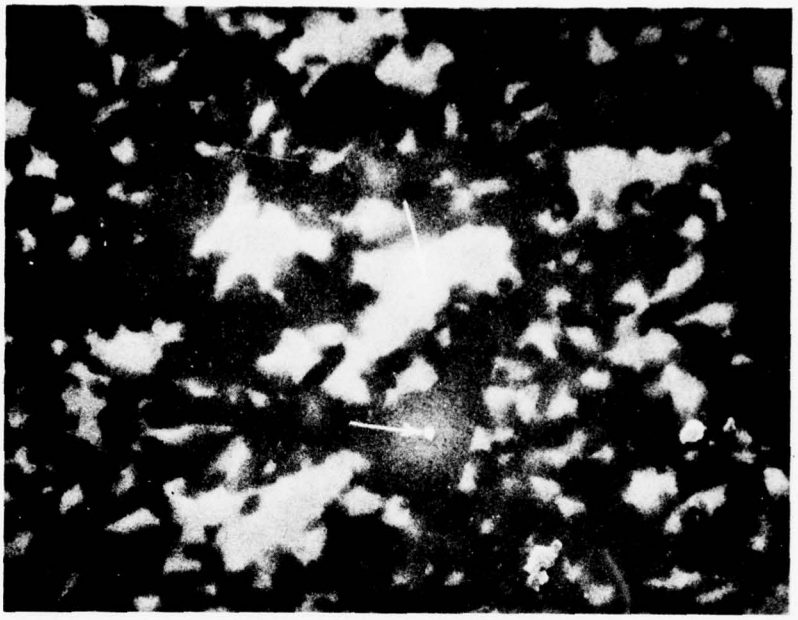

PL. 6138-3 4000X

Figure 13. SEM of Polished Section of Sample from Billet 1942 (25% Zyttrite Additive) used in Spot Scan Analysis.

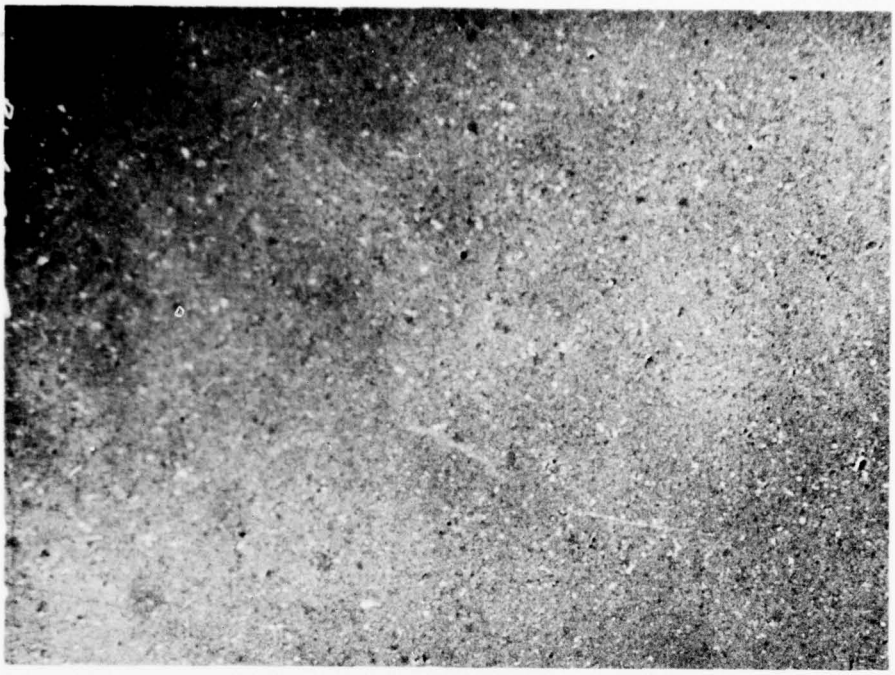

PL 6090-5 (a) 250X

Perpendicular to Hot Pressing Direction

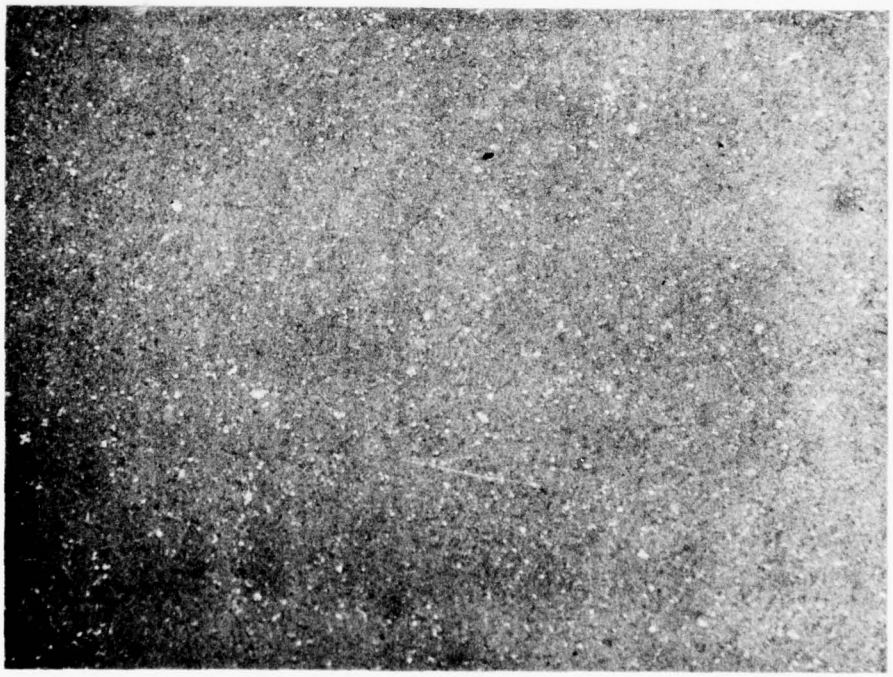

PL 6090-6 (b) 250X

Parallel to Hot Pressing Direction

Figure 14. Photomicrographs of Cross-Section of Billet of Norton NC-132 Grade Silicon Nitride.

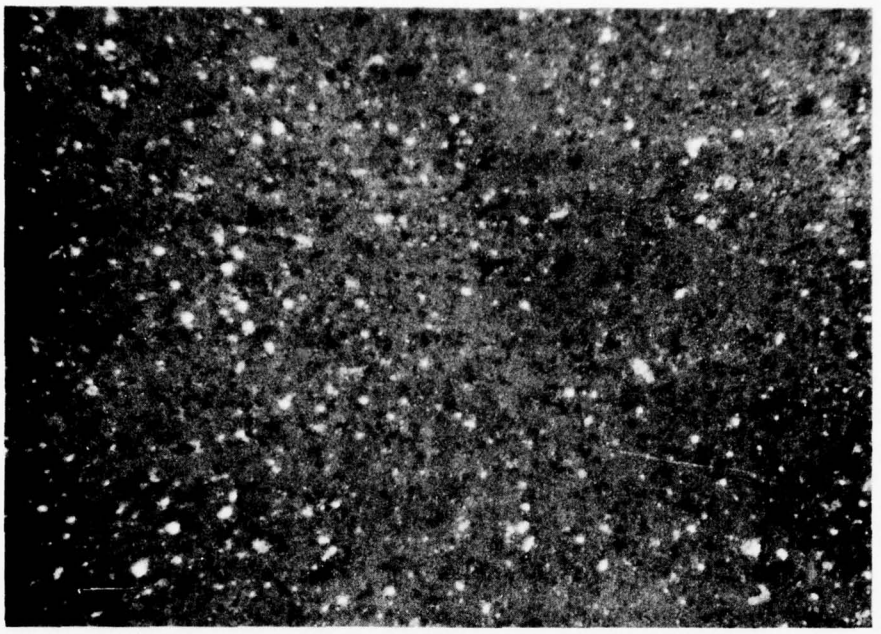

PL 6090-3 (a) 1000X

General Structure

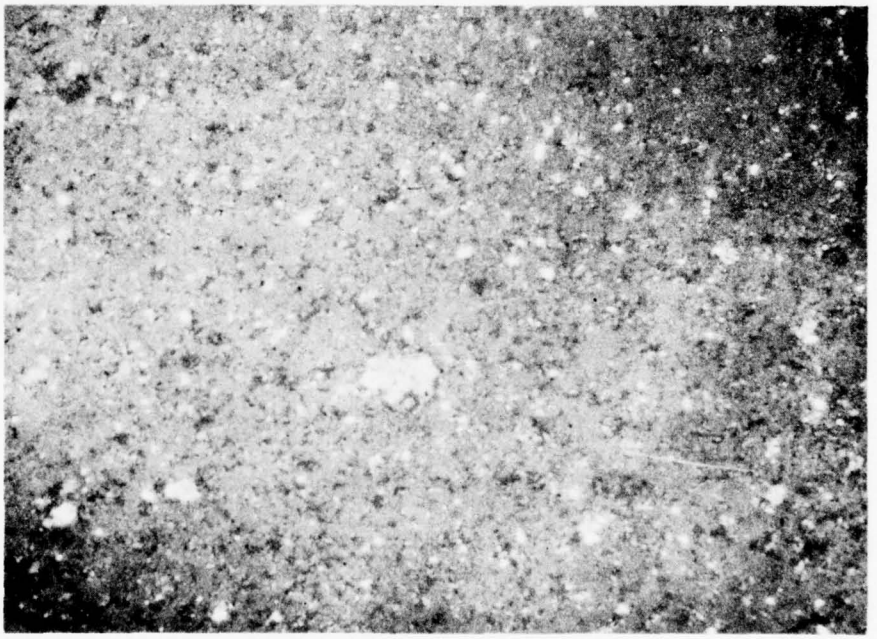

PL 6090-4 (b) 1000X

Selected Area Showing Large Second Phase Inclusion Particle

Figure 15. Photomicrographs of Cross-Section of Billet of NC-132 Silicon Nitride (higher mag. - 1000X).

X-ray Examination

Norton NC-132

The surface normal to the pressing direction of an NC-132 sample was directly examined with CuK α radiation without grinding into a powder. The values for 2 θ for the diffraction maxima, the interplanar spacing, d, computed from Bragg's Law and the observed peak intensity (100 = 500 counts/sec) were recorded. The pattern was explained in terms of three phases:

β -Si_3N_4 (major), α-Si_3N_4 and Si_2ON_2. The agreement between the interplanar spacing and that reported in the standard patterns was excellent.

In addition, an inverse pole-figure analysis of texture in the sample plane perpendicular to the pressing direction was performed for the β-Si_3N_4 component of an NC-132 sample. Comparison of the intensity for a consolidated microstructure with that of a random standard powder of the same material gives the relative orientation ("times random") of plane normals relative to a surface of interest. The ratios may be plotted on a stereographic projection to provide an "inverse pole figure".

Details of the inverse pole figure analysis are provided in Appendix I. The results showed the NC-132 sample had an essentially random texture.

Silicon Nitride-Zyttrite Compositions

X-ray diffraction analyses were performed on samples from billets representing each of the four compositions and the results are tabulated below.

TABLE IV

X-RAY ANALYSIS OF SI_3N_4-ZYTTRITE COMPOSITIONS

Billet	Composition	X-ray Diffraction Analysis
1937	10% Zyttrite addition	Primary phase is β Si_3N_4, no α phase, and 10 to 15% of zirconium oxynitride phase and about 5-10% silicon oxynitride phase (Si_2ON_2).
1938	15% Zyttrite addition	Primary phase is β Si_3N_4, no α phase, and about 20% of zirconium oxynitride phase and 5-10% of silicon oxynitride phase.
1936	20% Zyttrite addition	Primary phase is β Si_3N_4, no α phase, about 20 to 30% of zirconium oxynitride phase and about 10% of silicon oxynitride phase.
1939	25% Zyttrite addition	Primary phase is β Si_3N_4, no α phase, also about 25 to 35% of zirconium oxynitride phase $ZrO_2 - 2xN_{4x/3}$ (where $0.25 \leq x \leq 0.43$) as well as about 10% of silicon oxynitride phase.

Materials Evaluation

General

This portion of the program was concerned with an evaluation of the as-pressed billets and heat-treated, press-forged materials described in an earlier section. In addition, for comparison purposes, Norton Company's high purity silicon nitride composition NC-132 was also evaluated in terms of short term transverse bend strength tests, bend stress rupture tests, bend creep tests and tensile stress rupture tests.

Transverse Bend Strength

Short term 4-point bend tests were performed in air at temperatures up to 1370°C on specimens 4.45 cm x 0.51 cm x 0.25 cm (1 3/4" x .200" x .100") with an outer knife edge span of 3.81 cm (1.50") and an inner knife edge span of 1.27 cm (0.50") to ensure elastic bend conditions. A constant load rate was set to provide a nominal strain rate of about 10^{-4} sec^{-1}.

The results for all the fabricated materials and for the NC-132 material are documented in Table V, and reveal the effects of compositional and temperature variations.

The results show significantly lower low temperature strengths for the zyttrite containing samples as compared to NC-132 material. In particular, the average strength at room temperature for each zyttrite containing composition is approximately one-third lower than NC-132. This difference decreases with increasing temperature until at 1200°C there is reasonable equivalence between the 10, 20 and 25 wt. % zyttrite compositions and NC-132. It is at 1370°C, however, where the zyttrite containing compositions are superior (the 10 and 20 wt. % zyttrite compositions show strengths as much as double the NC-132 strengths).

The data are plotted as a function of temperature in Figure 16.

TABLE V

TRANSVERSE BEND STRENGTH RESULTS

Billet	Materials & Additives	Bend Strength, MN/m^2 (Kpsi) Rm. Temp.	1000°C (1832°F)	1100°C (2010°F)	1200°C (2192°F)	1370°C (2498°F)
1937	AME Si_3N_4 thru 15 μm	524 (76.2)	521 (75.7)	481 (69.9)	504 (73.3)	541 (78.6)
ρ = 3.23 g/cc	plus 10 wt. % Zyttrite-6	535 (77.8)	535 (77.7)	518 (75.3)	524 (76.1)	552 (80.2)
		538 (78.2)	516 (75.0)	496 (72.0)	541 (78.5)	526 (76.4)
		545 (79.2)	548 (79.6)	511 (74.2)	496 (72.1)	573 (83.2)
		561 (81.5)	566 (82.1)	492 (71.4)	552 (80.2)	546 (79.3)
1938	AME Si_3N_4 thru 15 μm	489 (71.1)	488 (70.9)	443 (64.4)	427 (62.0)	494 (71.6)
ρ = 3.40 g/cc	plus 15 wt. % Zyttrite-6	504 (73.2)	406 (58.9)	463 (67.2)	462 (67.1)	494 (71.7)
		528 (76.7)	436 (63.1)	421 (61.1)	450 (65.4)	469 (68.2)
		497 (72.2)	436 (63.4)	438 (63.8)	447 (64.9)	478 (69.4)
		511 (74.2)	455 (66.1)	457 (66.3)	476 (69.2)	481 (70.0)
1936	AME Si_3N_4 thru 15 μm	559 (81.2)	614 (89.3)	650 (94.4)	642 (93.1)	556 (80.8)
ρ = 3.49 g/cc	plus 20 wt. % Zyttrite-6	600 (87.1)	588 (85.3)	680 (98.9)	564 (81.9)	579 (84.1)
			544 (79.1)	676 (93.2)	621 (90.2)	590 (85.6)
1940	AME Si_3N_4 thru 15 μm	525 (76.3)	592 (86.0)	454 (66.0)	641 (93.1)	510 (74.1)
ρ = 3.50 g/cc	plus 20 wt. % Zyttrite-6	539 (85.6)	624 (90.7)	514 (74.6)	650 (94.5)	437 (63.5)
		565 (82.1)		594 (84.8)		574 (83.3)
						587 (85.2)
1939	AME Si_3N_4 thru 15 μm	568 (82.6)	595 (86.5)	564 (81.9)	581 (84.4)	438 (63.6)
ρ = 3.60 g/cc	plus 25 wt. % Zyttrite-6	538 (78.1)	526 (76.5)	539 (78.4)	595 (86.4)	433 (62.9)
		555 (80.6)	445 (64.7)	402 (73.0)	538 (78.2)	436 (63.4)
1942	AME Si_3N_4 thru 15 μm	603 (87.6)	635 (92.3)	689 (100.1)	527 (76.5)	406 (59.0)
ρ = 3.60 g/cc	plus 25 wt. % Zyttrite-6	610 (88.6)	586 (85.2)	507 (73.6)	610 (88.6)	444 (64.5)
					581 (84.4)	
1963	AME Si_3N_4 thru 15 μm	559 (81.2)				461 (67.0)
ρ = 3.54 g/cc	plus 20 wt. % Zyttrite-6	551 (80.0)				400 (58.2)
	(Forged)	562 (81.6)				463 (67.3)
		565 (82.1)				457 (66.4)
1964	AME Si_3N_4 thru 15 μm	545 (79.2)				554 (80.5)
ρ = 3.14 g/cc	plus 10 wt. % Zyttrite-6	525 (76.4)				511 (74.2)
	(Forged)	489 (71.2)				492 (71.5)
		565 (82.1)				558 (81.2)
						484 (70.4)
1965	AME Si_3N_4 thru 15 μm	505 (73.3)				282 (41.0)
ρ = 3.47 g/cc	plus 20% Zyttrite	310 (45.0)				320 (46.5)
	(Post-heat treated)	392 (57.0)				248 (36.0)
		421 (61.2)				290 (42.2)
1981	AME Si_3N_4 thru 15 μm	359 (52.1)				328 (47.5)
ρ = 3.24 g/cc	plus 10% Zyttrite	422 (61.2)				290 (42.1)
	(Post-heat treated)	333 (48.3)				272 (39.4)
		401 (58.1)				282 (40.8)
Norton NC-132	Norton Si_3N_4	915 (133.2)	810 (117.8)	611 (88.7)	553 (80.3)	288 (40.3
	MgO additive	724 (105.1)	528 (76.6)	687 (99.8)	540 (78.4)	274 (39.8)
		805 (117.0)	660 (95.9)	598 (101.4)	625 (90.8)	292 (42.4)
		772 (112.0)	830 (120.5)	747 (108.7)	637 (92.5)	260 (37.8)
			793 (115.1)	662 (96.1)		279 (40.6)

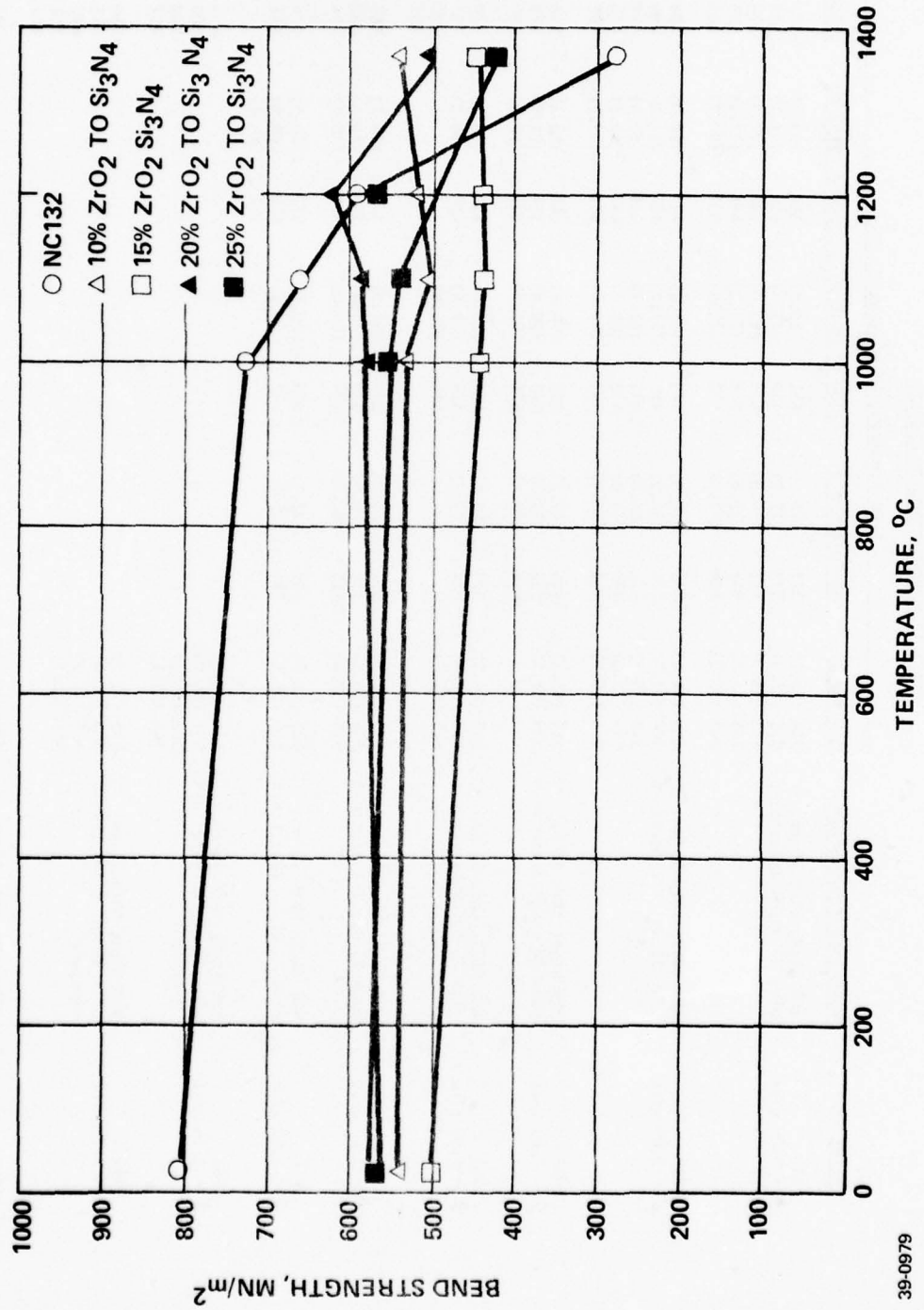
SHORT TIME BEND STRENGTH
○ NC132
△ 10% ZrO_2 TO Si_3N_4
□ 15% ZrO_2 Si_3N_4
▲ 20% ZrO_2 TO Si_3N_4
■ 25% ZrO_2 TO Si_3N_4
BEND STRENGTH, MN/m^2
1000
900
800
700
600
500
400
300
200
100
0
200
400
600
800
1000
1200
1400
TEMPERATURE, °C
39-0979

Figure 16.

The relatively low strengths observed below 1200°C may result from a number of possibilities as revealed from inspection of room temperature fracture faces of NC-132 and 10% zyttrite additive samples, Figures 17 and 18. Both structures appear to be composed of a duplex array of grain sizes, i.e., a small size and a larger size. The small size grains for the NC-132 sample are approximately 0.3 μm and the larger size grains are around 2 μm. In comparison, the small size grains for Billet 1937 material are 0.5 to 0.8 μm in size and the larger grains go to about 3 μm. Also, the grains in the zyttrite-containing sample show a more equiaxed structure.

Additional scanning electron microscopy evaluation of flaw sources was performed on R.T. test bars of Billets 1938, 1939, 1940 as well as 1937. In addition, an EDAX attachment to the microscope permitted qualitative chemical element determination down to the atomic number of sodium. The samples were coated with gold to prevent charging because silicon nitride is an insulator. Since the lines for gold overlapped those for zirconium, the sensitivity to zirconium was not as good as desired. Later, nickel coatings were employed at the expense of detail because of nickel oxidation.

Figure 19 shows a micrograph of the fracture face of a RT test bar of Billet 1937, which features a large grain in the internal structure which is rich in zirconium content and also showed molybdenum as a contaminating phase. A small number of these large particulates were found scattered throughout the fracture face.

Figure 20 shows a micrograph of the fracture face of a RT test bar of Billet 1938, which also shows a zone of large grains identified as being rich in zirconium content.

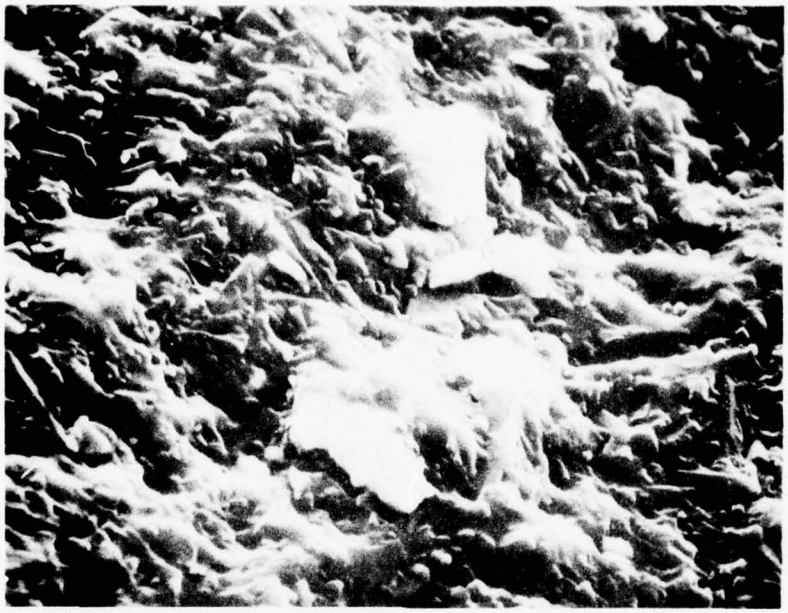

PL 6138-1 500X

Figure 17. Scanning Electron Micrograph of Fracture Face of R.T. Bend Test Bar of NC-132 Material.

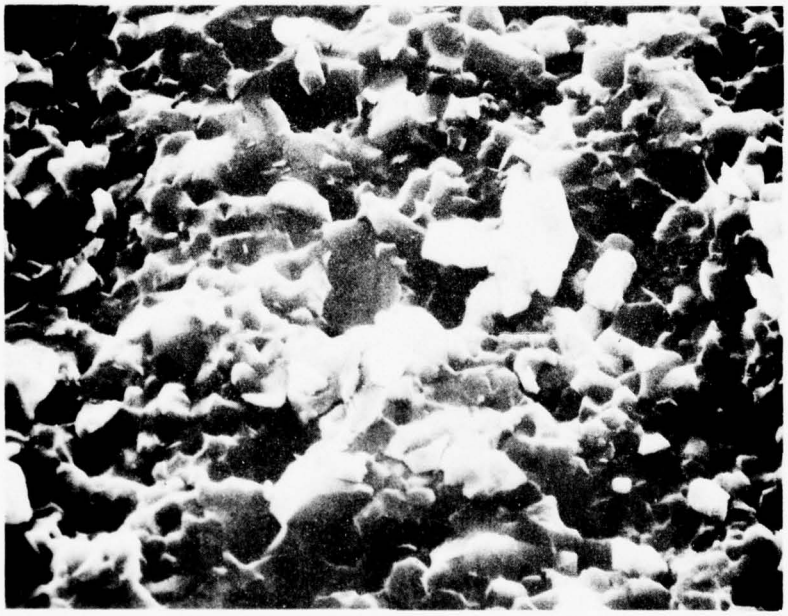

PL 6138-2 5000X

Figure 18. Scanning Electron Micrograph of Fracture Face of R.T. Bend Test Bar of Billet 1937 Material (10% Zyttrite Additive).

1937-2 2900X

Figure 19. Scanning Electron Micrograph of Fracture Face of R.T. Bend Test Bar of Billet 1937 Material (10% Zyttrite Additive) Featuring Large Grain with Zirconium and Molybdenum Content.

1938-4 3200X

Figure 20. Scanning Electron Micrograph of Fracture Face of R.T. Bend Test Bar of Billet 1938 Material (15% Zyttrite Additive) Featuring Zone of Large Grains Identified as Being Rich in Zirconium.

Figure 21 shows a micrograph of the fracture face of a RT test bar of Billet 1940 also revealing what appears to be a larger than average grain containing zirconiun near the tensile edge.

Figure 22 also shows a similar micrograph of a fracture face of a RT test bar of Billet 1939 revealing a zone of much larger than average grains rich in zirconium content. It is likely that these grains are the zirconium oxynitride phase identified previously in polished section micrographs. The fact that some of this phase is in the form of such large grains may be important in hindering the achievement of higher bend strengths.

Overall, however, the EDAX measurements revealed that the microstructure and chemistry was rather uniform. In traverses across the microstructure of the different test bar fracture faces, the silicon peak was always greater than the gold-zirconium peak and there was never a large variation in the ratio of the silicon peak to gold-zirconium. This indicates a rather uniform distribution of two principal elements in the structures.

Auger spectroscopy determinations were not very enlightening. This technique measures the composition of the first few atom layers, so the samples could not be coated prior to analysis. The samples were previously notched (saw-cut about 30% through the thickness) cleaned, then fractured in air immediately before loading in the vacuum chamber. Thus, a nearly clean fracture surface was provided for examination.

In principal, the Auger unit beam size can be reduced to about 1/4 μm. However, the uncoated samples became so badly charged that SEM pictures with any resolution could not be obtained and detailed analyses were not possible. Basically, the elements Si, N, O and C were observed in

1940-6 8300X

Figure 21. Scanning Electron Micrograph of Fracture Face of R.T. Bend Test Bar of Billet 1940 Material (20% Zyttrite) Showing a Larger than Average Grain Containing Zirconium.

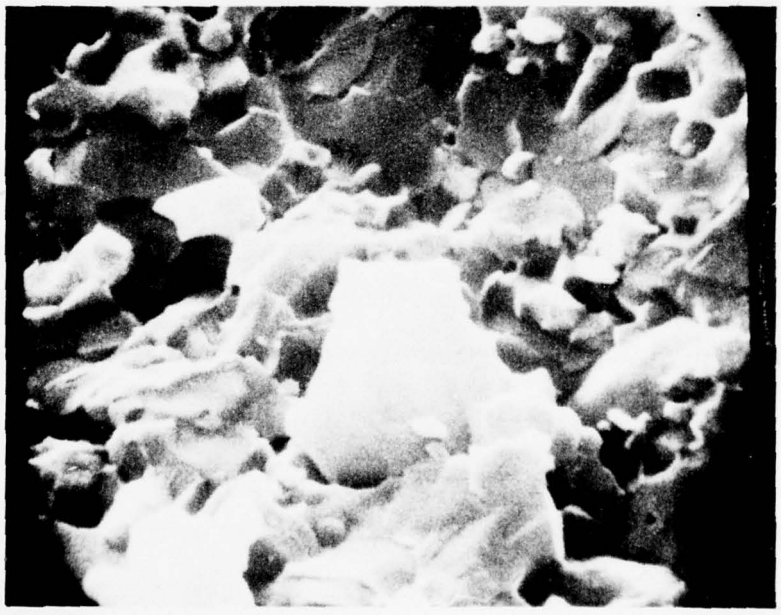

1939-8 8900X

Figure 22. Scanning Electron Micrograph of Fracture Face of R.T. Bend Test Bar of Billet 1939 Material (25% Zyttrite) Showing Large Grains of Zirconium Containing Material.

the various samples. The C content was measured lower after sputtering or long pumpting time and, therefore, was mostly (or all) contamination from vapor in the vacuum chamber. Some oxygen could also be adsorbed from the atmosphere. Information on spatial distribution was not attainable. The ratios of the O:Si:N peaks appeared uniform from comparing the various samples. Zirconium was only barely detectable (one small peak and the other major peak not evident in background). The one zirconium peak qualitatively increased going from 10% → 15% → 20% → 25%.

The NC-132 sample shows a significant population of elongated grains that are characteristic for this material. Intergranular fracture of a material containing elongated grains can lead to a much rougher surface with a higher specific surface area relative to an equiaxed microstructure. Thus, the more irregular fracture surface topography of the material containing the elongated grain structure may be one reason for its higher fracture energy.

At high temperatures, e.g., 1370°C, however, fracture behavior for these materials appears dominated by the nature of intergranular chemistry and/or phases. The data for the current program support the findings of the previous effort, that the zyttrite additive has a positive effect in substantially raising the high temperature strength of silicon nitride. In substituting a zirconium oxynitride phase for a silicate phase containing magnesium as often used for silicon nitride densification purposes, a more refractory material less likely to exhibit liquid formation has been positioned as a discreet phase as well as intergranularly in the silicon nitride microstructure. The failure mechanism at such temperatures has become as much, if not more, a function of intergranular phase characteristics than silicon nitride morphology. In this instance, at 1370°C the bend

strengths of the 10 and 20 wt. % zyttrite-containing samples are approximately double that of the NC-132 samples. It is not clear why the 15 and 25 wt. % zyttrite-containing samples did not perform as well. Forged zyttrite-containing samples did not show the promise originally anticipated as the room temperature and 1370°C data for samples from Billet 1963 and 1964 show no improvement over samples not forged. It was anticipated that a preferred orientation of the plate-like matrix grains of silicon nitride could provide enhanced strengthening.

Figures 23 and 24 are scanning electron micrographs at 5000X of RT fracture faces for each of these forged compositions. Grain enlargement based on average grain size measurement (10% zyttrite additive) is observed in Billet 1964 with some texture apparent in Billet 1963 (20% zyttrite additive). Polished section micrographs of samples from Billets 1964 and 1963 are given in Figures 25 and 26. Scattered concentrations of large grain size zirconium oxynitride phase appear in the microstructure of Figure 25. In Figure 26, a small amount of porosity is evident (estimated at about 2%).

Post-heat treatment to enlarge grains further was carried out in the case of Billet 1965 (20% zyttrite additive) and Billet 1981 (10% zyttrite additive). It was considered that the enlarged grain size might further improve the high temperature strength. However, the results demonstrate a reduction in strength in both test temperatures, possibly from expansion anisotropy of the various phases.

The microstructures for each of these billets is depicted in Figures 27 and 28. The average grain sizes for both samples was 4-6 μm.

Polished section micrographs of a cross-section of Billets 1965 and 1981 are given in Figures 29 and 30.

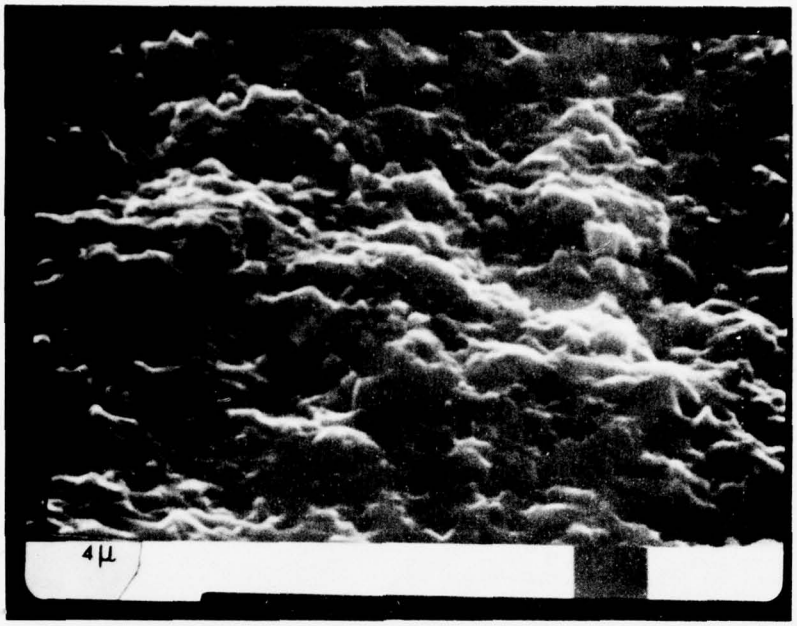

Figure 23. Scanning Electron Micrograph of Fracture Surface of R.T. Bend Test Bar from Billet 1963 (Forged 20 Wt. % Zyttrite Additive).

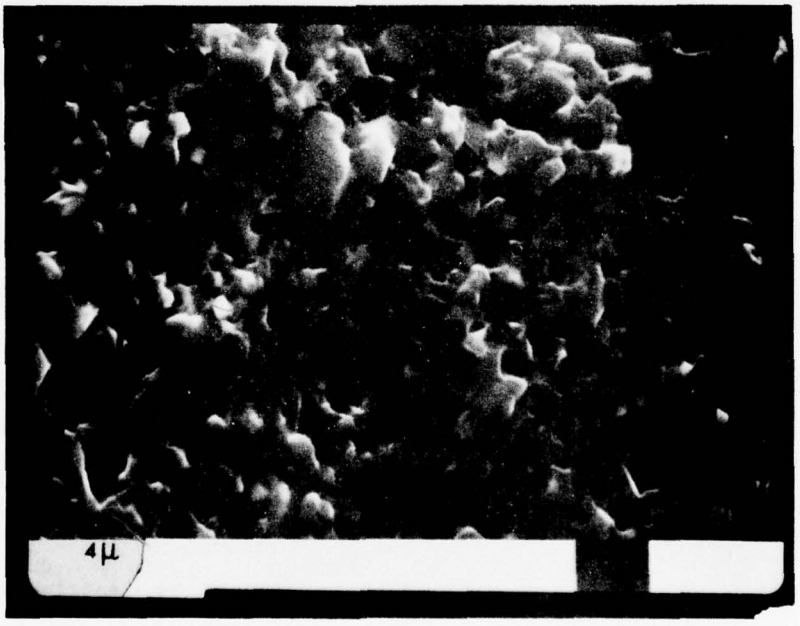

Figure 24. Scanning Electron Micrograph of Fracture Surface of R.T. Bend Test Bar from Billet 1964 (Forged 10 Wt. % Zyttrite Additive).

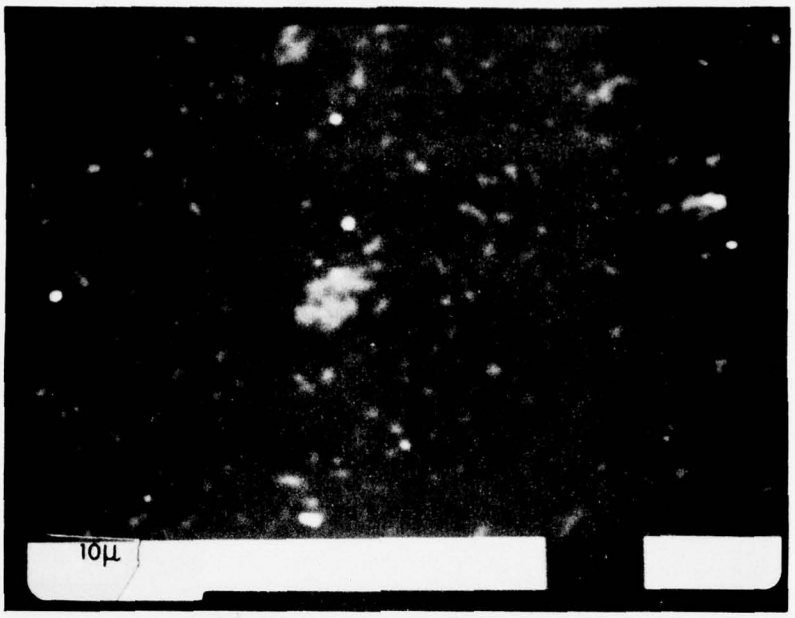

1400X

Figure 25. Polished Section Micrograph of Sample Cross-Section from Forged Billet 1964.

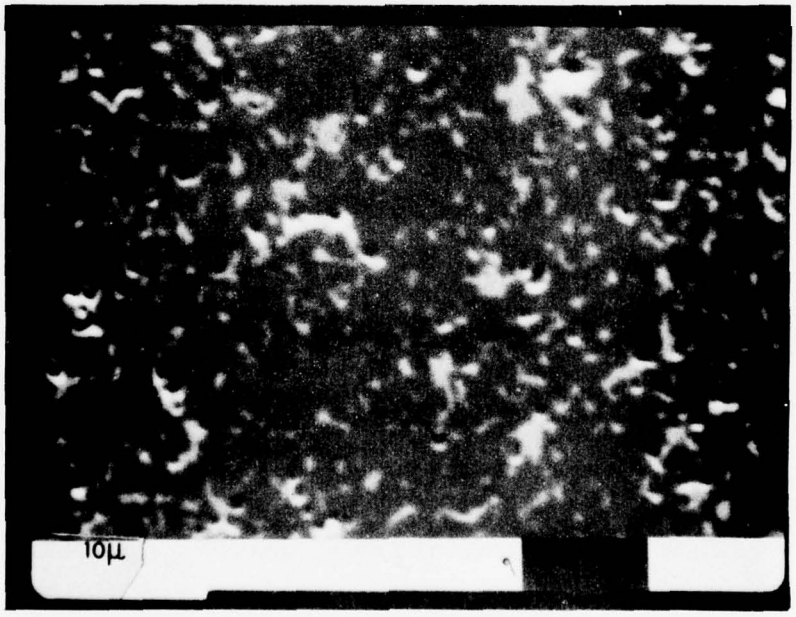

1800X

Figure 26. Polished Section Micrograph of Sample Cross-Section from Forged Billet 1963.

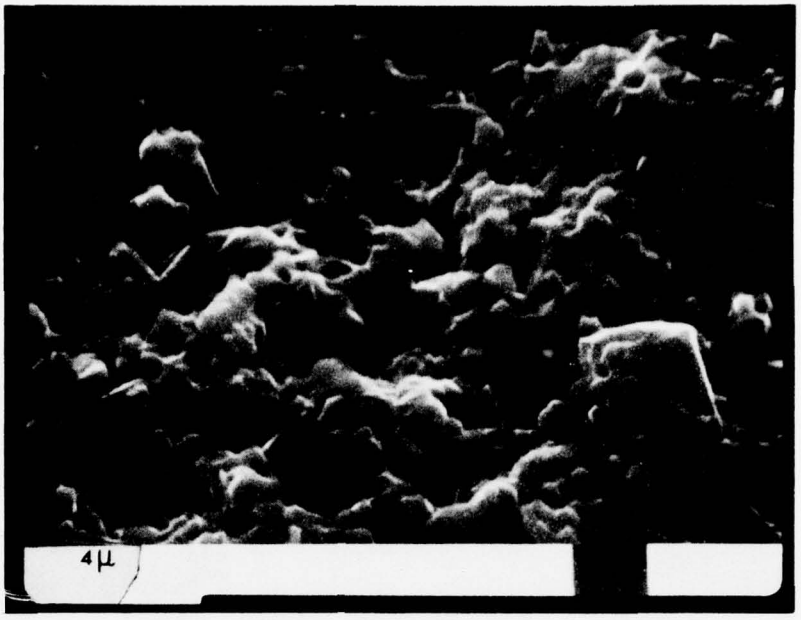

Figure 27. Scanning Electron Micrograph of Fracture Surface of R.T. Bend Test Bar from Billet 1965 (Post-heat Treated, 20 Wt. % Zyttrite Additive).

Figure 28. Scanning Electron Micrograph of Fracture Surface of R.T. Bend Test Bar from Billet 1981 (Post-heat Treated, 10 Wt. % Zyttrite).

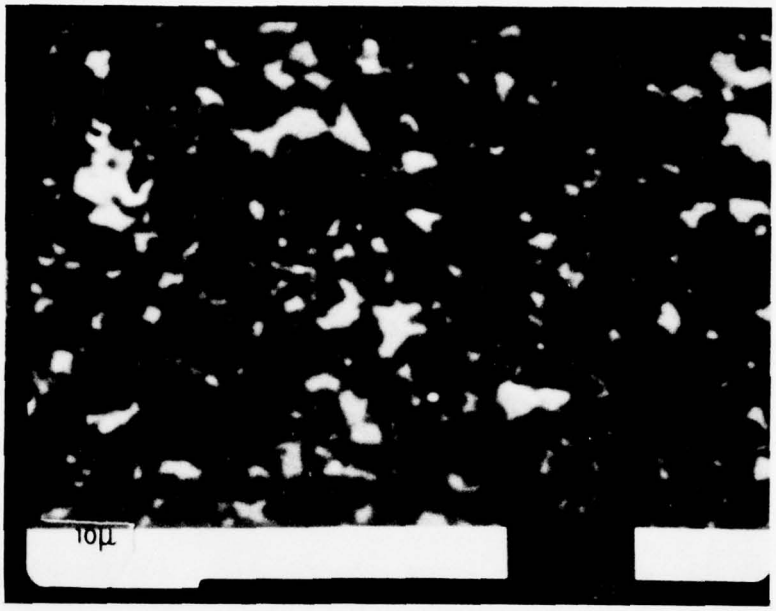

Figure 29. Polished Section Micrograph of Cross-Section of Sample from Billet 1965 Showing Granular Development of Zirconium Oxynitride Phase.

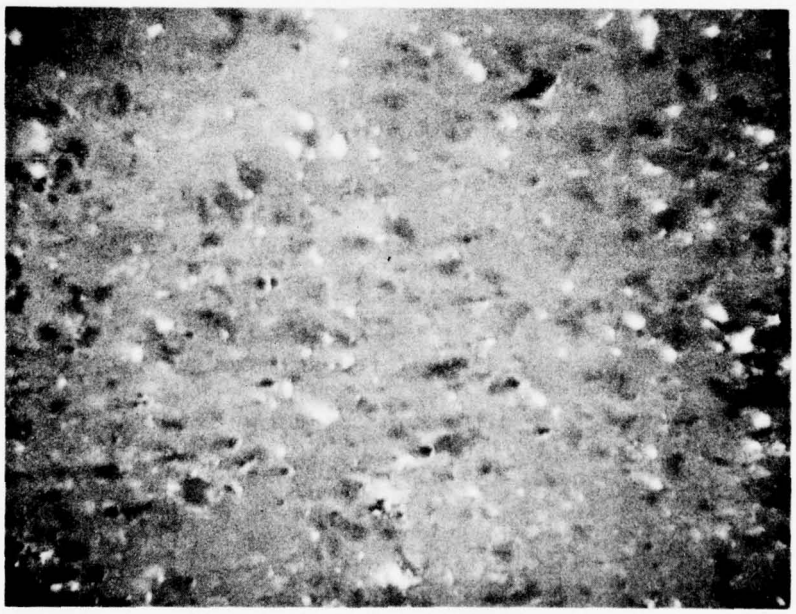

1000X

Figure 30. Polished Section Micrograph of Cross-Section of Sample From Billet 1981.

On the basis of the overall bend test data, it was decided to select the 10 and 20 wt. % zyttrite compositions for further evaluation in bend stress rupture and best creep testing.

Bend Stress Rupture Evaluation

Testing was conducted in air under a 4-point bending mode using silicon carbide for knife edge fixtures. The test specimen dimensions were 4.45 cm x 0.51 cm x 0.25 cm (1 3/4" x 0.100" x 0.200") with an outer span of 3.81 cm (1.500") and an inner span of 1.27 cm (0.500"). A predetermined load was applied smoothly in a few seconds with a cam actuator on the load bearing lever arm. A cut-off switch clock circuit connected to the lever arm was utilized to detect and record failure.

The results were determined using the elastic beam formula:

$$\sigma = \frac{3Pa}{bh^2}$$

where σ = transverse rupture strength in psi,

P = load in pounds required to fracture,

b = specimen width in inches and,

h = specimen thickness in inches

For a dead load test where plastic deformation occurs, an indication of the deviation from this formula can be obtained from the approximate equation for the steady-state stress:

$$\sigma = \frac{Pa}{bh^2} \quad (2 + m)$$

where m is the strain rate sensitivity exponent. For metals, m is typically 0.2 to 0.3 so the stress will drop from its initial value to a value near that given by the above equation. For ceramics, m is typically between

0.5 and 1.0 so that there is often only a small difference between the actual steady-state stress and the calculated elastic stress. Cracking and cavitation, however, will invalidate this relation.

The bend stress rupture results are tabulated in Table VI for the 10 and 20 wt. % zyttrite containing compositions and for NC-132 material. They are also graphically depicted as dotted lines in Figures 31 to 33 to reflect no failure in many cases. The results show a strong stress sensitivity for both zyttrite containing compositions at the 276 MN/m^2 (40 Kpsi) level with the exception of the test conducted at 1200°C for a sample from Billet 1960 (10% zyttrite additive). This sample did not fail at the end of 110 hours in contrast to the two samples from Billet 1959 (20% zyttrite additive) which failed at the end of 3.9 and 13.7 hours. The NC-132 material showed similar stress sensitivity at high stress levels, but deformed readily at lower stress and intermediate temperature. Strain measurements were performed on cool-down on the tested samples to assess relative deformation behavior and these data are given in Table VI.

Scanning electron micrographs of fracture surfaces of ruptured samples, in general, reveal rather extensive grain growth of corrosion reaction products (zirconium and silicon oxides) developed during cool-down in the air atmosphere. This is particularly striking when oxidized tensile surfaces of intact specimens are examined as shown in Figures 34 and 35. Figure 34 shows a SEM of the surface of an NC-132 sample exposed at 1370°C under 8 Kpsi for 101 hours. The reaction product surface grain size is ten times that of the NC-132 grain size. Figure 35 shows a SEM of the surface of a sample from Billet 1959 exposed at 1370°C under 8 Kpsi for 160.8 hours. It shows the outline of a thin-cracked large grain reaction product structure apparently superimposed over residual fine-grain Si_3N_4 structure.

TABLE VI

BEND STRESS RUPTURE RESULTS FOR Si_3N_4

Billet	Material	Temperature °C	Temperature °F	MN/m^2	(Kpsi)	Time To Failure (Hours)
1959	AME Si_3N_4 thru 15 um plus 20 wt. % Zyttrite-6	1370	(2498)	276	(40)	2.1
1959	"	1370	(2498)	172	(25)	171.8 - did not fail; 0.47% strain
1959	"	1370	(2498)	55	(8)	160.8 - did not fail; 0.27% strain
1959	"	1285	(2345)	276	(40)	9.0, 0.31% strain
1959	"	1285	(2345)	172	(25)	150 - did not fail; 0.35% strain
1959	"	1285	(2498)	55	(8)	148.3 hrs. - did not fail
1959	"	1200	(2192)	276	(40)	3.9, .13% strain
1959	"	1200	(2192)	276	(40)	13.65, .11% strain
1959	"	1200	(2192)	172	(25)	132.1 hrs. - did not fail; .23% strain
1960	AME Si_3N_4 thru 15 um plus 10 wt. % Zyttrite-6	1370	(2498)	276	(40)	0.47
1960	"	1370	(2498)	172	(25)	110.5 - did not fail; .27% strain
1960	"	1370	(2498)	55	(8)	161.7, did not fail; 0.06% strain
1960	"	1285	(2345)	276	(40)	14.2 - .24% strain
1960	"	1285	(2345)	172	(25)	180.2 - did not fail; .25% strain
1960	"	1200	(2192)	276	(40)	112 - did not fail; .18% strain
1960	"	1200	(2192)	172	(25)	134.4 hrs. - did not fail; .19% strain
1960	"	1285	(2345)	55	(8)	127.2 hrs. - did not fail
NC-132	Norton Co.	1200	(2192)	276	(40)	5.5, .32% strain
NC-132	"	1285	(2345)	276	(40)	0.2
NC-132	"	1285	(2345)	172	(25)	12.7 - sample did not fail by fracture, but deformed extensively triggering micro-switch, 1.53% strain
NC-132	"	1200	(2192)	172	(25)	145 hrs. shutdown with .63% strain
NC-132	"	1370	(2498)	55	(8)	101 hrs. - 2.5% strain
NC-132	"	1370	(2498)	276	(40)	Instant failure
NC-132	"	1370	(2498)	172	(25)	0.1

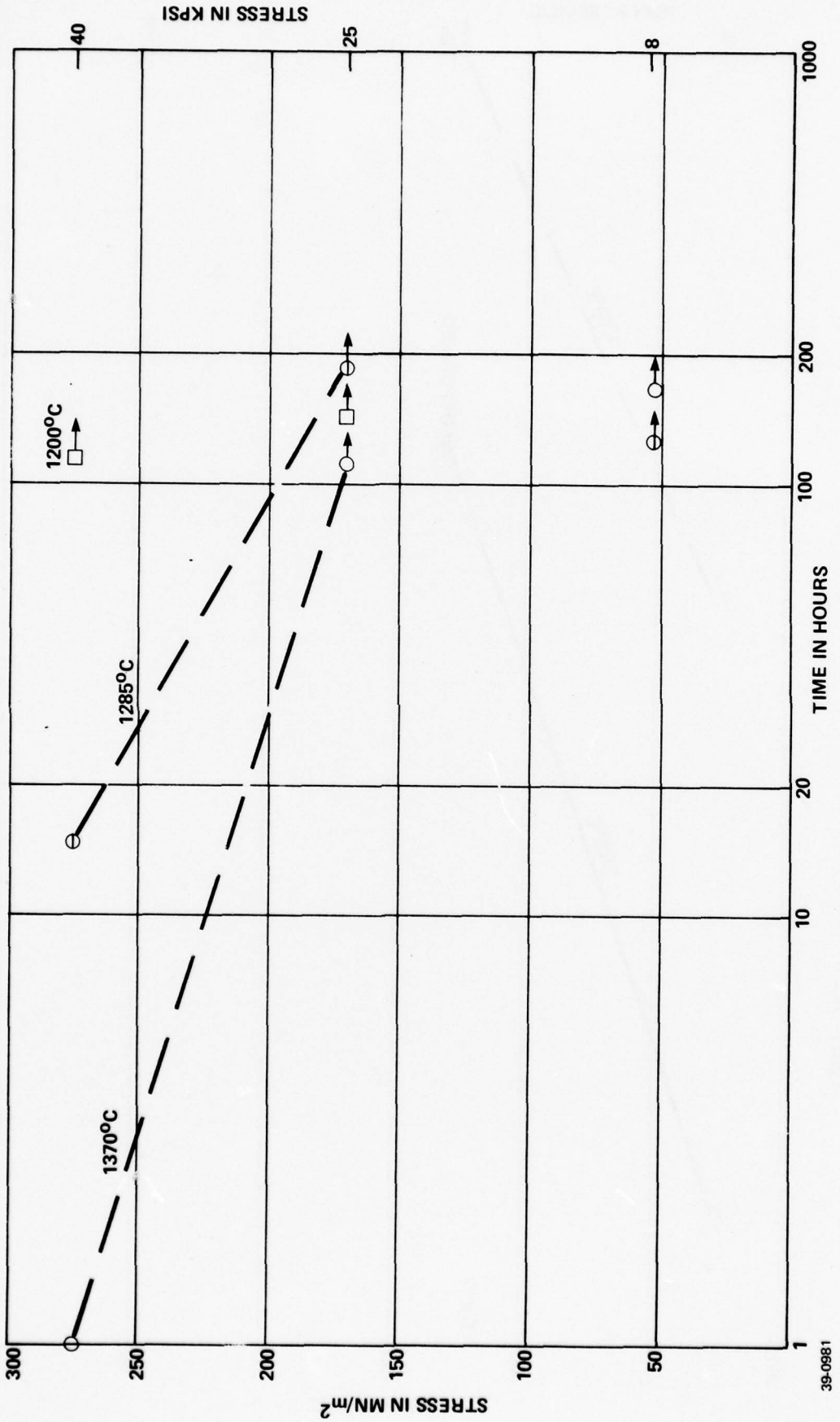

Figure 31. BEND STRESS RUPTURE PLOTS FOR Si_3N_4 BILLET 1960 (10 W/O ZYTTRITE ADDITIVE) BARS

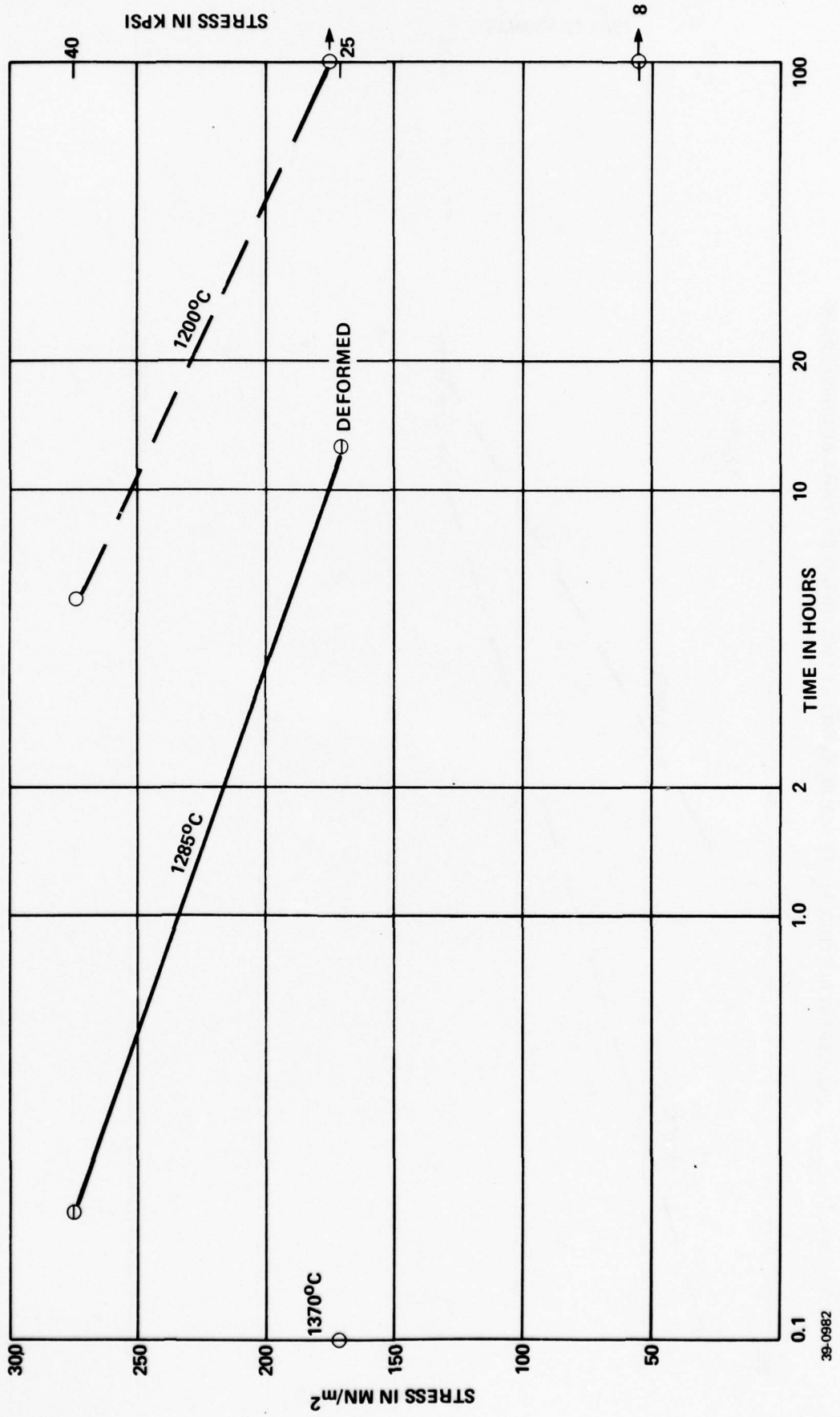

Figure 32. BEND STRESS RUPTURE POLTS FOR NC 132 BARS

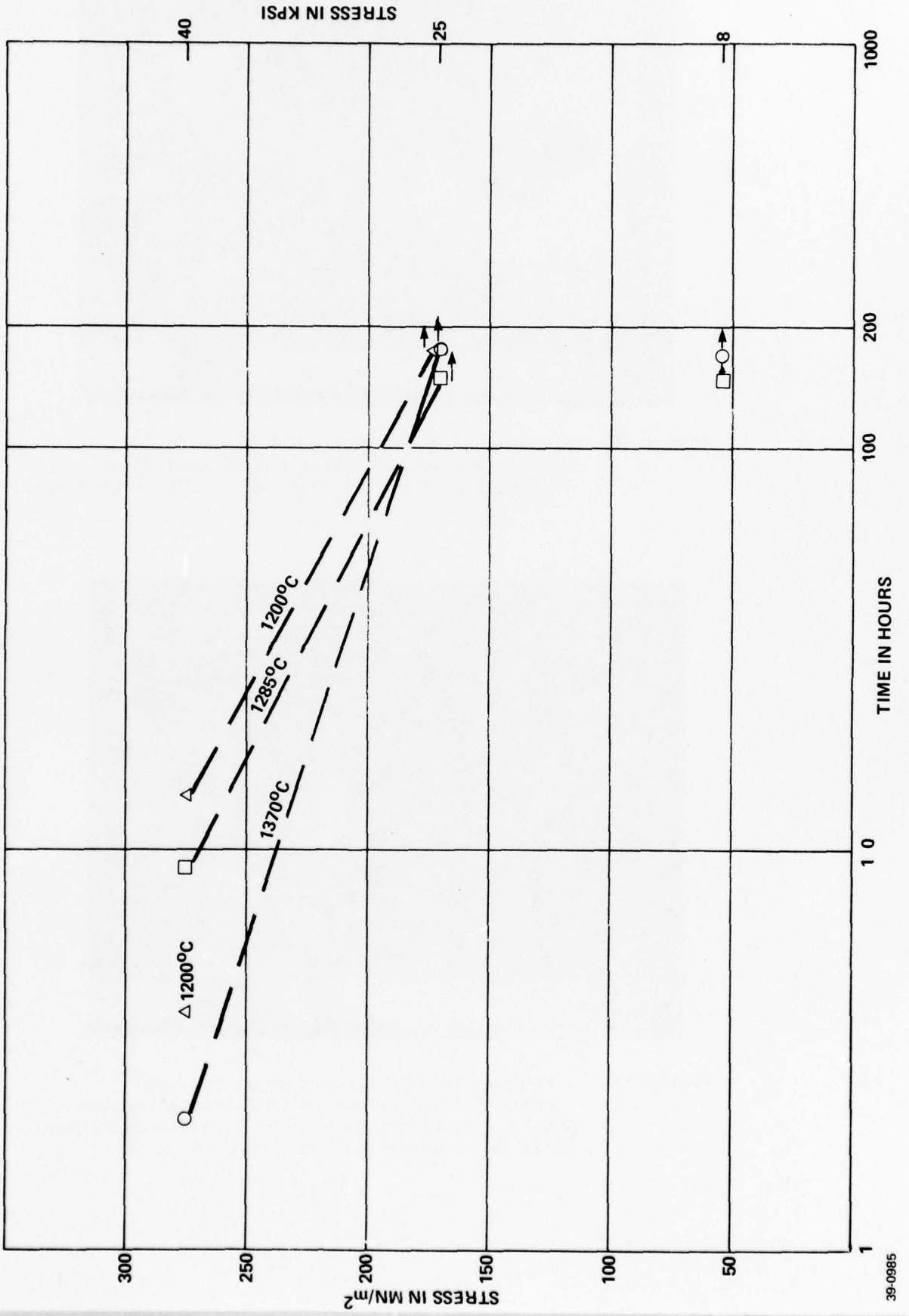

Figure 33. BEND STRESS RUPTURE POLTS FOR Si_3N_4 BILLET 1959 (20 W/O ZYTTRITE ADDITIVE) BARS

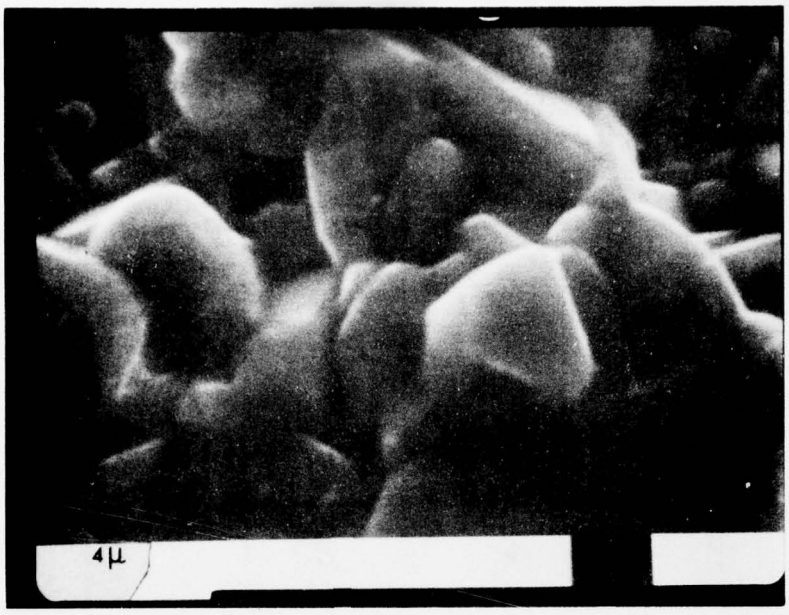

Figure 34. Scanning Electron Micrograph of Oxidized Tensile Surface of Intact NC-132 Bend Stress Rupture Bar after 101 Hours at 1370°C under 8 Kpsi.

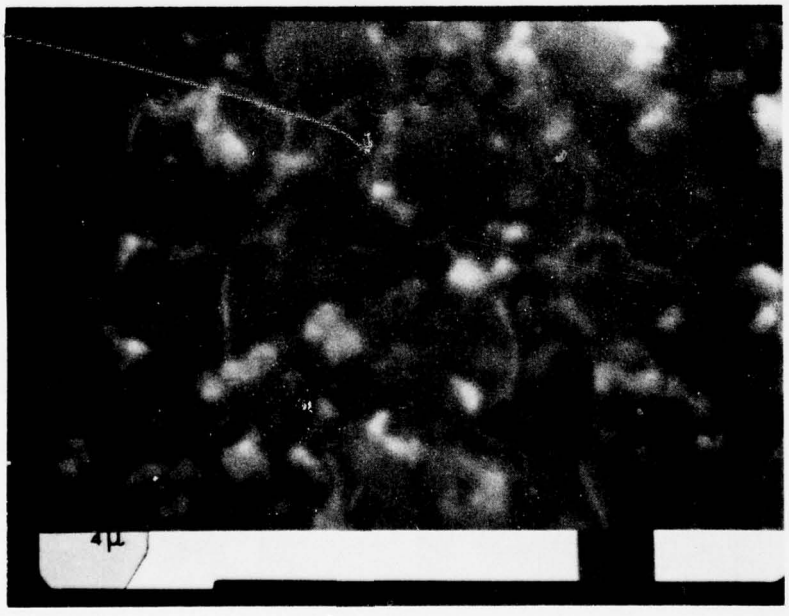

Figure 35. Scanning Electron Micrograph of Oxidized Tensile Surface of Intact Bend Stress Rupture Sample from Billet 1959. (20% Zyttrite Additive) after 160.8 Hours at 1370°C under 8 Kpsi.

Creep in Bending

Creep testing in bending was performed with an evaluation of the Norton NC-132 material as well as samples from Billet 1960 (10% zyttrite additive) at a test temperature of 1370°C. Testing was conducted in air under a 4-point bending mode using silicon carbide knife edge fixtures. The specimen dimensions were identical to those for specimens used in stress rupture testing and were 4.45 cm x 0.51 cm x 0.25 cm (1 3/4" x 0.100" x 0.200").

Alumina loading tubes and the carbide knife edge fixtures are employed in a constant load device. Creep strain was determined with center point deflection transmitted by a sapphire rod to an LVDT which was referenced to the knife fixture through a spring-loaded support tube. Load was determined from the output of a calibrated load cell and load deflection traces were transmitted to x-y recorders.

Table VII provides the results for the two compositions evaluated at 1370°C. For the NC-132 material at stress levels above 172 MN/m^2 (25,000 psi), no significant creep strain measurements could be measured because of essentially immediate fracture. The value of $1.3 \times 10^{-6}/_s$ for a load of 170 MN/m^2 (24,700 psi) is apparently anomalous to the value of $2.0 \times 10^{-6}/s$ for a load of 128 MN/m^2 (18,500 psi). However, this may result from a transient creep strain phenomenon caused by grain boundary liquid in NC-132 material at this temperature being squeezed out during alternating stress intervals, i.e., one specimen provided 3 measurements at alternate stress levels. A second sample tested at 170 MN/m^2 (24,700 psi) provided a creep strain rate measurement of 2.5 x 10-6/s.

The data for samples from Billet 1960 (10% zyttrite additive) reveal rather promising creep stability for this class of material. The creep rate

TABLE VII

RESULTS OF BEND CREEP MEASUREMENTS ON NC-132 AND BILLET 1960

(10 Wt. % Zyttrite) at 1370°C)

Material	NC-132	NC-132	NC-132	NC-132	1960	1960	1960
Applied Load, MN/m^2 (psi)	241 (35,000)	170 (24,700)	128 (18,500)	76 (11,000)	426 (61,800)	328 (47,600)	248 (36,000)
Strain Rate (per sec)	No measurement	1.3×10^{-6}	2.0×10^{-6}	9×10^{-7}	2×10^{-7}	3.4×10^{-8}	1×10^{-8}
	Immediate fracture	2.5×10^{-6}*					

*A second sample used to check apparently anomalous measurement of 1.3×10^{-6} creep strain rate.

appears to be at least 2 orders of magnitude less than for NC-132. Creep strains were recorded at loads up to 426 MN/m^2 (61,800 psi). The measured creep strain rates of 10^{-8} per sec were really beyond the precision limits of the equipment employed, and it was decided to perform additional measurements at 1450°C where more deflection was anticipated. In this instance, samples from Billet 1959 (20% zyttrite additive) and 1960 (10% zyttrite additive) were evaluated along with NC-132 material. The data are tabulated in Table VIII. Again, the creep rate for the zyttrite-containing compositions were about two orders of magnitude less than for the NC-132 material.

The data plotted as steady-state strain rate vs. log stress in Figures 36 and 37 indicate a low exponent for the relation $\dot{\varepsilon} = \sigma^{\eta}$, where $\dot{\varepsilon}$ is the strain rate, σ is the stress and η an exponent determining process mechanism. An exponent of $\eta < 2$ usually indicates a visco-elastic mechanism, i.e., a glassy phase diffusional creep or grain boundary sliding. The slopes of the plots in Figure 36 is approximately 2 and it is likely that the deformation mechanism is diffusional creep through a glassy phase or grain boundary sliding, depending on the viscosity of a grain boundary glassy phase. The slope of about 4 for the bend creep plot at 1370°C (Figure 37) probably reflect cavitation or cracking as a mechanism. The data for NC-132 appear consistent with that reported for NC-132 type material in the literature.[4] The higher viscosity of the grain boundary phase in the zyttrite-containing materials probably accounts for the enhanced creep resistance. In addition, data for tensile creep tests described below are included in Figure 37 for discussion in the next section.

Tensile Stress Rupture Testing

A limited number of tensile stress rupture tests were performed on NC-132 and silicon nitride-10% zyttrite additive materials. The samples were of

TABLE VIII

RESULTS OF BEND CREEP MEASUREMENTS ON NC-132
AND SAMPLES FROM BILLETS 1959 AND 1960 AT 1450°C

Material	1959 (20% Zyttrite)	1959	1959	1960 (20% Zyttrite)	1960	1960	NC-132	NC-132
Applied Load, MN/m^2 (psi)	190 (27,500)	252 (36,550)	327 (47,400*)	172 (24,500)	252 (36,600)	317 (45,900*)	68 (9,800)	150 (21,700*)
Creep Strain Rate, (per sec)	1.7×10^{-8}	9.0×10^{-8}	6.7×10^{-8}	1.35×10^{-8}	2.7×10^{-8}	4.4×10^{-8}	4.31×10^{-6}	2.42×10^{-5}

Figure 36. BEND CREEP STRAIN RATE VS. STRESS FOR NC132 BARS & BARS FROM BILLETS 1959 (20 W/O ZYTTRITE ADDITIVE) & 1960 (10 W/O ZYTTRITE ADDITIVE)

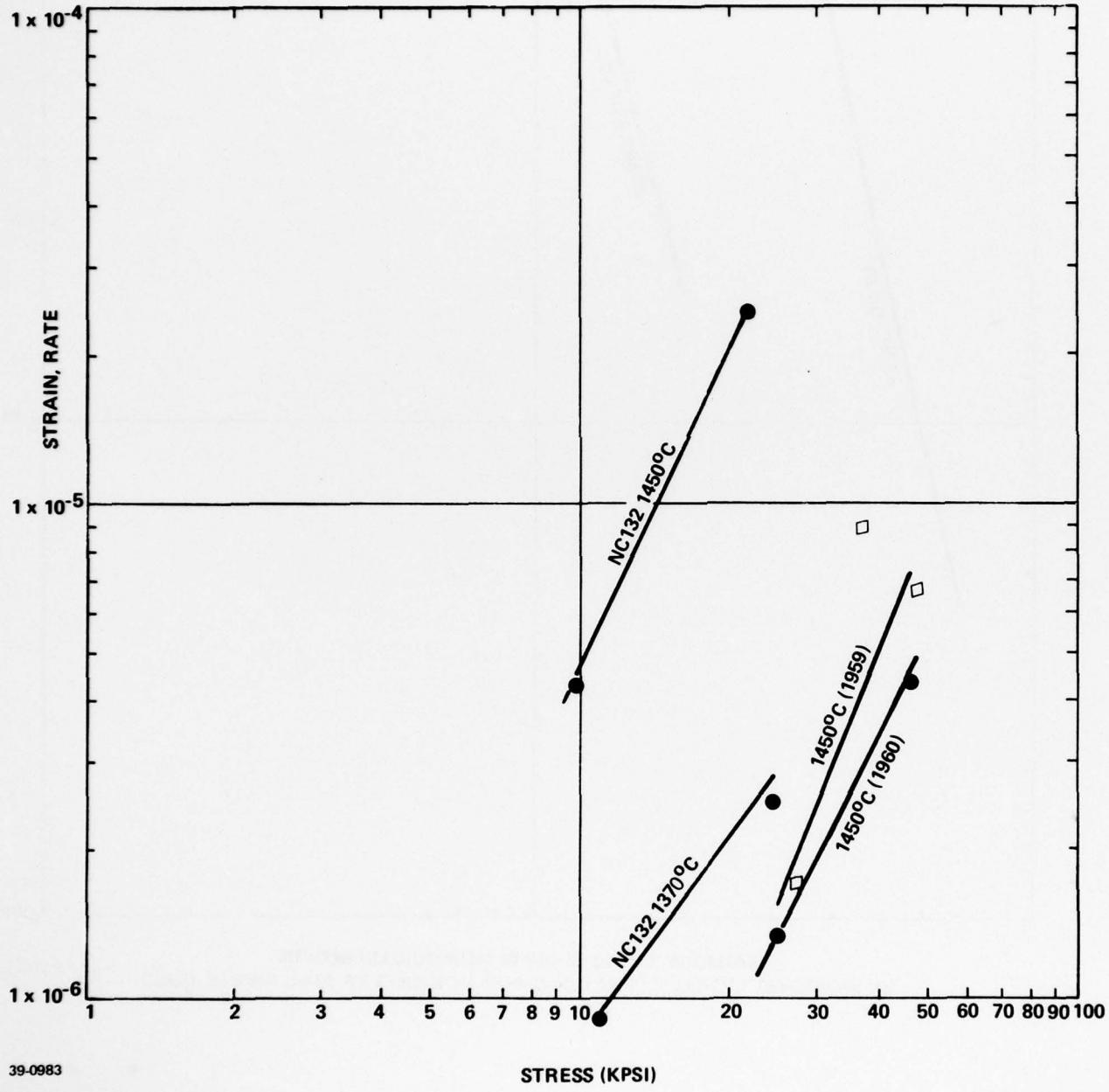

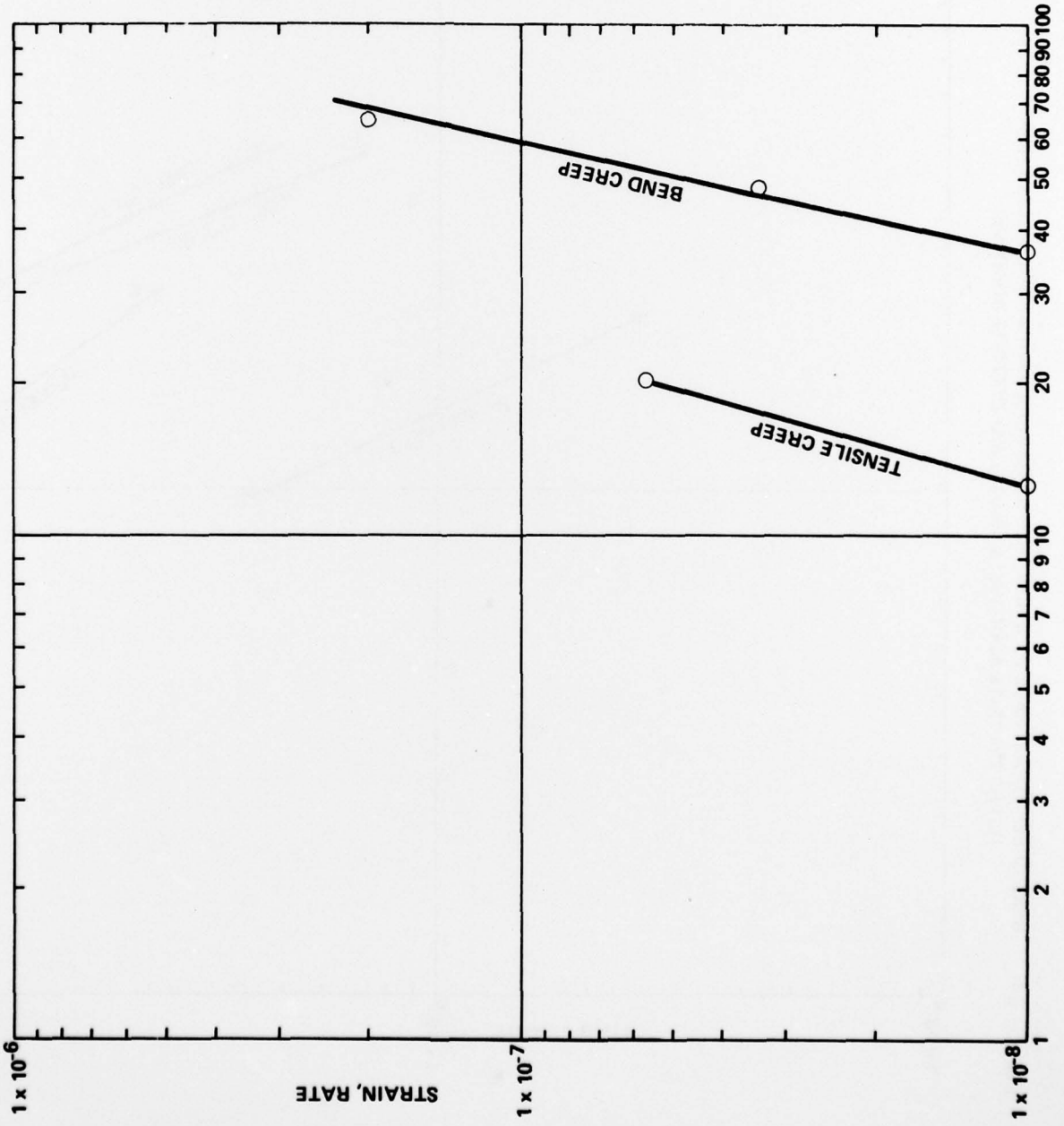

Figure 37. CREEP STRAIN RATE VS. STRESS AT 1370°C FOR BEND & TENSILE SPECIMENS OF SILICON NITRIDE WITH 10 W/O ZYTTRITE ADDITIVE

cylindrical dogbone shape 10.16 cm (4 inch) in total length, 5.08 cm (2 inch) gage length, 0.58 cm (0.23 inch) gage diameter.

The samples were tested in a platinum wire tube furnace using a Riehl Creep frame unit under static load conditions. The high temperature zone of the furnace allowed uniform heating of the 5.08 cm (2 inch) gage length of the samples in an air atmosphere.

The silicon nitride-10% zyttrite additive test bars were machined from a large hot pressed billet 13.3 cm (5 1/4 inch) x 13.3 cm (5 1/4 inch) x 1.27 cm (1/2 inch thick. The hot press conditions duplicated those for the smaller billets and the billet density was measured as 3.23 g/cc.

The NC-132 samples were cut from a 15.2 cm (6 inch) x 15.2 cm (6 inch) x 1.59 cm (.625 inch) billet obtained from the Norton Company.

Table IX provides the results of the tensile stress rupture tests performed.

The results appear to support the contention that values of tensile strength measurements for ceramics are often about one-half those obtained in bending. This is believed to arise from the larger volume of material under tension in tensile testing. At any rate, the data reveal again the superiority of the zyttrite containing composition at elevated temperature. The two tensile creep strain rate numbers calculated from strain measurements of the 10% zyttrite composition at 1370°C have also been plotted in Figure 37 and it is interesting to note that if the applied stresses for the bend creep plot were halved, then the bend creep plot would be approximately identical to the tensile creep plot. The deformation mechanism in either case appears the same and with the high slope value of about 4, must be associated with cavitation or microstructure cracking.

TABLE IX

TENSILE STRESS RUPTURE RESULTS FOR 10% ZYTTRITE-SILICON NITRIDE AND NC-132 MATERIALS

Sample No.	Composition	Test Temp. °C	Applied Stress MN/m^2	(Kpsi)	Time to Failure Hrs.	Plastic Strain %	Strain Rate
1	10% Zyttrite-Si_3N_4	RT	258	37.4	0	0	-
2	10% Zyttrite-Si_3N_4	1370	138	20.0	3.1	.065	5.8×10^{-8}
3	10% Zyttrite-Si_3N_4	1370	86.	12.5	102-no break	0.37	1.0×10^{-8}
4	10% Zyttrite-Si_3N_4	1285	138	20.0	34.3	.06	4.9×10^{-9}
5	10% Zyttrite-	1200	138	20.0	.2	-	-
6	NC-132	RT	335	48.6	0	0	-
7	NC-132	1370	138	2.0	0	0	-
8	NC-132	1370	86.	12.5	.1	-	-

CONCLUSIONS

Yttria-stabilized zirconium oxide additons to high purity silicon nitride improve the high temperature strength, stress rupture and creep properties of hot pressed samples very markedly.

At room temperature, however, the average bend strengths of the four (4) compositions evaluated are each about one-third lower than Norton Company's NC-132 silicon nitride composition. This difference decreases with increasing temperature until at 1200°C there is reasonable equivalence between the 10, 20 and 25 wt. % zyttrite compositions and NC-132 in terms of short-time bend strength measurements.

At 1370°C, the zyttrite containing compositions (10 and 20 wt. % additions) show short time bend strengths as much as double those of the NC-132 material.

The high temperature strength appears related to the high temperature stability of intergranular or grain boundary phases. The resulting zirconium oxynitride phase in zyttrite-containing compositions appears much more refractory than a counterpart phase in NC-132 material.

Bend stress rupture results for 10 and 20 wt. % zyttrite-containing compositions show a strong stress sensitivity at the 276 MN/m^2 (40 Kpsi) level, above 1200°C. The NC-132 material shows similar stress sensitivity at high stress levels, but deforms readily at lower stress and intermediate temperatures. At a stress of 172 MN/m^2 (25 Kpsi) both zyttrite containing compositions survived well over 100 hours exposure in an air atmosphere with less than 0.5 percent strain.

Creep in bending measurements show that at 1370°C the creep rate for the 10% zyttrite additive composition is at least two orders of magnitude

less than for NC-132. At 1450°C, the observed creep rate is also about two orders of magnitude lower than NC-132 material for both 10 and 20 wt. % zyttrite compositions.

All compositions appear to follow deformation kinetics related to a visco-elastic mechanism, i.e., glassy-phase diffusional creep or grain boundary sliding.

Tensile stress-rupture test measurements performed on 10% zyttrite and NC-132 compositions (5.08 cm (2 inch)) gage length, (.58 cm (.23 inch)) gage diameter, shows values approximately one-half those obtained in bending. The superiority of the zyttrite-containing composition is consistent in these tests.

REFERENCES

1. T. Vasilos and R.M. Cannon, Jr., "Improving the Toughness of Refractory Compounds," NASA-CR-134813 (1975).

2. D.J. Shanefield and R.E. Mistler, "Filter for Ceramic Slips," Bull. Am. Ceram. Soc., Vol. 55, No. 2, p. 213 (1976).

3. F. Lange, Zirconium Additions to Silicon Nitride, Presented at Fall Meeting of Am. Ceram. Soc., 1978.

4. A. McLean et al, Brittle Materials Design, High Temperature Gas Turbine, AMMRC-CTR-73-9, March 1973.

APPENDIX I

The diffraction intensities obtained by reflection from a surface oriented normal to the pressing direction of Norton Company NC-132 silicon nitride was recorded in Table A-1. Those maxima belonging to the β-Si_3N_4 component have been extracted and are summarized in Table V. A portion of this sample was pulverized in a PICA blender mill and used to prepare a diffraction pattern for a randomly oriented powder. The general agreement with the standard powder diffraction pattern, Table A-1, supports the assumption that the orientation of grains in the powder is random. As the peak widths in the consolidated NC-132 and the powder are identical, peak heights rather than integrated intensities were compared.

The ratio of the intensity of the consolidated sample to that of the random powder, I/I_{random}, is presented for each set of diffracting planes in the last column of Table A-2. The texture is extremely weak and virtually non-existent: The "times random" orientation ranges from a minimum of 0.40 to a maximum of 1.36. The extreme values are, for the most part, obtained for the weak intensities with large uncertainties.

To minimize the effect of uncertainty in the measurement of intensity, those intensities which were greater than 20% of the maximum intensity in the pattern, I(210), were extracted from Table A-1.

hkl	I/I_{random}
100	0.80
110	1.00
200	1.05
101	1.23
210	1
301	0.92
321	1.25
411	1.04

TABLE A-I

X-RAY DIFFRACTION ANALYSIS OF PHASES PRESENT IN NORTON NC 132 TEST BAR

						Standard Pattern 9-259 β-Si_3N_4 Hexagonal a=7.603, c=2.909 Å			Standard Pattern 9-250 α-Si_3N_4, Hexagonal a=7.758, c=5.623			Standard Pattern 17-545 Si_2ON_2, Orthorhombic a=5.473, b=8.843, c=4.835 Å		
2θ	d(Å)	I	I/I_{max} (β-Si_3N_4)	I/I_{max} (α-Si_3N_4)	I/I_{max} (Si_2ON_2)	d(Å)	I/I_{max}	hkl	d(Å)	I/I_{max}	hkl	d(Å)	I/I_{max}	hkl
13.40	6.607	9.3	21.6			6.63	17	100						
18.97	4.678	2.3			19.5							4.66	80	110
19.97	4.446	11.8			100							4.43	100	020
20.55	4.322	6.3		61.2					4.32	50	101			
22.90	3.883	3.6		35.0					3.88	30	110			
23.33	3.813	14.3	33.2			3.82	20	110						
26.47	3.367	6.2		60.2	52.5				3.37	30	200	3.36	100	111
27.03	3.299	39.8	92.3			3.31	85	200						
31.01	2.884	7.2		70.0					2.893	85	201			
31.55	2.836	4.3		41.7					2.823	5	002			
32.62	2.745	3.4			28.8							2.74	20	200
33.67	2.662	16.2	37.6			2.668	100	101						
34.52	2.598	9.5		92.2	80.5				2.599	75	102	2.61	50	130
35.40	2.536	10.3		100.					2.547	100	210			
35.62	2.520	15.9												
36.02	2.493	43.1	100			2.492	100	210						
37.69	2.387	2.6			22.0							2.39	40	201
38.98	2.311	5.0	11.6		98.3	2.312	9	111	2.320, 2.312	60, 8	211, 112	2.30	30	131
40.30	2.238	4.3		41.7					2.244	5	300	2.22	10	040
41.40	2.181	6.6	15.3			2.180	35	201						
41.93	2.155	3.3		32.0					2.158	30	202	2.16	10	112
42.90	2.108	5.5			46.6							2.10	10	221
43.51	2.080	3.2		31.1					2.083	55	301			
46.87	1.938	2.7		26.2					1.937	2	220			
47.82	1.902	4.0	9.3			1.904	5	220						
48.05	1.893	2.5	5.8			1.892	5	211						

TABLE A-I (Concl'd)

2θ	d(Å)	I	I/I_{max} (β-Si_3N_4)	I/I_{max} (α-Si_3N_4)	I/I_{max} (Si_2ON_2)	d(Å)	I/I_{max}	hkl	d(Å)	I/I_{max}	hkl	d(Å)	I/I_{max}	hkl
48.30	1.884	10.4		100					1.884	8	212			
49.93	1.826	5.9	13.7			1.827	20	310						
52.19	1.753	12.7	29.5			1.753	70	301						
57.90	1.593	5.9	13.7			1.593	20	221	1.596	35	222			
60.00	1.542	2.3	5.3			1.548	9	311	1.542	5	320			
61.40	1.510	7.5	17.4			1.512	35	320	1.507	8	213			
62.50	1.486	2.7							End of Reported Pattern					
64.05	1.454	4.3	10.0			1.455	35	002						
64.90	1.437	6.6	15.3			1.437	20	410						
65.82	1.419	3.0												
66.55	1.405	2.5	5.8			1.358	3	112						
70.20	1.341	15.5	36.0			1.341	40	321						
70.85	1.330	2.3	5.3			1.330	17	202						
71.60	1.318	3.3	7.7			1.317	17	500						
73.45	1.289	10.5	24.4			1.288	85	411						
75.02	1.266	4.5	10.4			1.268	20	330						
75.70	1.256	4.5	10.4			1.255	85	212						
77.08	1.237	2.3	5.3			1.244	3	420						

TABLE A-II

INVERSE POLE FIGURE ANALYSIS OF TEXTURE PERPENDICULAR TO PRESSING DIRECTION OF β-Si_3N_4 COMPONENT OF NORTON NC-132 SILICON NITRIDE

Standard Pattern 9-259			NC-132 Random Powder		Normal to Pressing Direction		
hkl	d(Å)	I/I_{max}	d(Å)	I/I_{max}	d(Å)	I/I_{max}	I/I_{random}
100	6.63	17	6.64	27.0	6.61	21.6	0.80
110	3.82	20	3.82	33.2	3.81	33.2	1.00
200	3.31	85	3.30	87.7	3.30	92.3	1.05
101	2.668	100	2.666	83.1	2.662	37.6	1.23
201	2.492	100	2.494	100	2.493	100	1.00
111	2.312	9	2.320	25.9	2.311	11.6	0.45
201	2.180	35	2.183	28.9	2.181	15.3	0.53
220	1.904	5	1.902	8.7	1.902	9.3	1.07
211	1.892	5	-	-	1.893	5.8	-
310	1.827	20	1.828	11.7	1.826	13.7	1.17
301	1.753	70	1.754	31.9	1.753	29.5	0.92
221	1.593	20	1.595	13.6	1.593	13.7	1.01
311	1.548	9	1.541	6.8	1.542	5.3	0.78
320	1.512	35	1.511	12.8	1.512	17.4	1.36
002	1.455	35	1.454	21.8	1.454	10.0	0.46
410	1.437	20	1.437	17.2	1.437	15.3	0.89
112	1.358	3	-	-	-	-	-
321	1.341	40	1.341	28.9	1.341	36.0	1.25
202	1.330	17	1.326	6.0	1.330	5.3	0.88
500	1.317	17	1.316	9.3	1.319	7.7	0.83
411	1.288	85	1.290	23.4	1.289	24.4	1.04
330	1.268	20	1.267	10.4	1.266	10.4	1.00
212	1.255	85	1.256	19.9	1.256	10.4	0.52
420	1.244	3	1.237	13.1	1.237	5.3	0.40

The two reflections 100 and 200 correspond to first and second order reflections from the same set of planes, and thus should give the same "times random" ratio. The average, $0.92 \pm .12$ provides a measure of the uncertainty in these ratios, and indicates no texture within experimental error. The difference between the intensity ratio may be explained in terms of a 10% uncertainty in estimation of peak height which is not unreasonable.

As the microstructure has essentially random texture, the labor of computing a stereographic projection of normals to the diffracting planes for preparation of an inverse pole figure was not justified. The texture in several important zones, however, was examined.

For (hol) planes parallel to 010:

(100), (200)	I/I_{random} =	$0.92 \pm .12$
(101), (202)		$1.05 \pm .18$
(301)		0.92

For (hkl) planes parallel to 110:

(110), (220)	I/I_{random} =	$1.03 \pm .03$
(221)		1.01

For (hkO) planes parallel to 001:

(100), (200)	I/I_{random} =	$0.92 \pm .12$
(110), (220)		$1.03 \pm .03$
(310)		1.17
(320)		1.36
(410)		0.89
(330)		1.00
(420)		$0.40 \pm .40$

Variation of "times random" orientations of planes whose normals fall in these zones display no systematic variation. All ratios are close to unity and, as mentioned above, it was concluded that the microstructure displayed no signifiant texture.